# Modelling the evolution of flowering time in perennial plants

Patricia Morris

Thesis submitted to the Faculty of Science in partial fulfillment of the requirements
for the degree of
Master of Science Mathematics and Statistics[1]

Department of Mathematics and Statistics
Faculty of Science
University of Ottawa



[1]The M.Sc. program is a joint program with Carleton University, administered by the Ottawa-Carleton Institute of Mathematics and Statistics

# Abstract

The onset of flowering time in a plant is extremely significant when evaluating population success. Floral growth, seed production, and dispersal are all dependent upon flowering time. Flowering early (and hence longer) increases the prospect of pollination but typically reduces vegetative growth and yields fewer/smaller flowers. Flowering late (and hence shorter) guarantees more/bigger flowers but carries the risk of insufficient pollination. This fundamental trade-off between growth and flowering time suggests that there may be an optimal time to initiate flowering. In this thesis, we consider a deterministic hybrid integrodifferential model where we represent the growing season in continuous time and the time between seasons as a discrete map. We track the evolution of flowering time, as a phenotype, by explicitly considering it as a variable in our model. The model is analyzed from two different viewpoints: (1) by mutual invasion analysis in the sense of adaptive dynamics; and (2) by deriving equations for the mean trait value and total population density when flowering time is considered to be Gamma-distributed. In both cases evolution to an intermediary flowering time was observed.

# Dedications

To my parents, Warren and Debbie Morris, who have always supported me. I wouldn't be who I am today without you. To my grandparents, Wayne and Nadia Morris, for believing that I could do anything. Your memory forever gives me strength.

# Acknowledgement

I would like to thank my supervisor, Dr. Frithjof Lutscher, for his guidance and support throughout this project. I would also like to thank the University of Ottawa for their financial assistance.

# Contents

# List of Figures

# List of Tables

# Chapter 1

# Introduction

## 1.1 Biological background

Plant population growth is dependent upon flower production, pollination, and successful seed germination. All of these dynamics occur during the growing season, when environmental conditions are suitable for plant activity. During the growing season, plants are faced with the question of how to allocate resources towards biomass growth, flowering, and seed production. Early flowering increases the time available for pollination and seed production. However, there is evidence that plant size influences reproductive success, with larger plants generally producing a greater number of seeds [1]. This observation suggests that flowering early may be detrimental if plant biomass is small. Alternatively, late flowering allows for larger plant biomass and thus increased seed production, but the time remaining for pollination and seed germination is limited. These advantages and disadvantages for early and late flowering suggest that there could be an optimal time during the season for a plant to flower. Examining this trade-off between plant size and seed development is the motivation for this thesis.

During the growing season, plants initiate flowering at a particular time. At the onset of flowering, plants begin allocating resources from their own growth and survival to reproduction and offspring development [33]. Plants that flower too early less time to grow and will have a smaller size during the reproductive phase, fewer resources to allocate to floral growth, and thus produce fewer seeds. Alternatively, later flowering allows for more resources allocated to plant growth and seed development, but shortens the time available for floral pollination, seed dispersal and germination [11]. This observation describes the fundamental trade-off between plant size and seed development [4]. Plants also assortatively mate by flowering time; early flowering plants will mate disproportionately with other early flowering plants, while late blooming plants will mate disproportionately with late bloomers [37]. The tradeoff between growth and flowering, along with assortative mating, suggests that plant

density may be higher when flowering begins midway through the season.

The time that flowering begins is particularly important when climate change is taken into account. In an environment with a rapidly changing climate, the length of the growing season can vary unexpectedly from year to year. As a consequence, plants that previously flowered at a suitable time may become maladapted to their environment. For instance, if the growing season unexpectedly increases in length, a plant that previously flowered at a suitable time one year may then flower too early the next year. Alternatively, plants that previously flowered too late may now flower at a suitable time if the growing season lengthens. The ability of a plant population to survive such variation depends upon the evolutionary properties of the plant.

This thesis considers the evolution of flowering time for a fixed growing season. We hypothesize that, over time, the flowering time of a perennial plant population will evolve to reach an intermediary value within the growing season. To test this hypothesis, we model the evolution of flowering time as an explicit variable.

Different models for flowering time have been studied in the past. Many of these models have been statistical in nature, relying on experimental data [11, 25, 27, 35]. Some probabilistic models track the genetic allelles that code for flowering time and evaluate fitness under various methods of selection [16, 38], while others construct so-called integral projection models to make predictions using the life-history of the plant [22, 28]. Flowering time is also often modelled using a quantitative genetics approach, where analysis is done on the phenotypic correlation between parents and offspring [19, 21, 37]. We construct a novel deterministic hybrid integrodifferential model with flowering time as a variable. We analyze our model using adaptive dynamics and by tracking the mean trait value and population density. We detail these methods and the required theory in the next two sections.

## 1.2 Methods

We create a mathematical model to track the population density of a perennial plant over time. We explicitly consider flowering onset as a variable in our model and examine the density of flowers with respect to this trait. Due to the dynamics of perennial plants, we create a hybrid model across two time scales. We track floral growth, death, and pollination during the growing season in continuous time using an integrodifferential equation. Plant survival and seedling success between seasons is represented in discrete time using a recursion equation, which includes the solution of the within-season equation.

We analyze the evolution of flowering onset in our model using two different methods: (1) mutual invasion analysis in the sense of adaptive dynamics; and (2) reduction to a model for the mean trait value and total density of the population. For both methods, we perform numerical simulations wherein we iterate the updating function of the model until the system reaches a steady state. We consider the system

to have reached a steady state when the difference in population density between subsequent years is less than a predefined, very small threshold. We compare our results for both methods.

The adaptive dynamics method requires significant theory, which we present in the next section. We outline the background behind the approach, and give examples of a simple and slightly more complex application. Both examples refer to purely continuous models, as this is the type of model the theory is most often applied to. Hence, the application to our hybrid model will differ slightly from the examples given. Subsequent to the adaptive dynamics section, we present our motivation for choosing this formulation, alongside an example for finding the equilibrium values of a simple hybrid model.

## 1.3 Adaptive dynamics

### 1.3.1 Background and Invasibility Analysis

Adaptive dynamics is a theoretical approach for studying some of the phenotypic changes that take place in an evolving population [36]. A phenotype is an observable characteristic or trait of an organism such as flowering time in plants or the colour of a rabbit's coat. Adaptive dynamics aims to study the evolution of traits that specifically affect fitness. Fitness, in this context, measures reproductive success in the population. Although an organism's phenotype is in part determined by its genotype, adaptive dynamics does not consider the genetic level and instead focuses on how the ecological interaction of individuals within a population affects the evolution of the phenotype. This approach allows for the approximation of complicated genetic interactions using simpler models [10]. In the simplest case, adaptive dynamics considers a single phenotypic trait, represented by a one-dimensional variable. Many extentions of this theory have been developed, but we will focus only on this simple scenario.

If the mutation rate for a phenotype is sufficiently low, it can be assumed that the population reaches its ecological attractor before a new phenotype appears within the population [26, 29]. Hence, we assume a separation of time scales such that ecological dynamics take place on a fast time scale while evolutionary dynamics are slow [5]. We also assume that mutations are rare and have small phenotypic effects [12, 26]. Given the rarity of mutation, it is typical to initially focus on a population with only one phenotype at ecological equilibrium. Such a population, consisting of only one phenotype, is called *monomorphic*. Reproduction is assumed to be both asexual and clonal so that every offspring is phenotypically identical to its parent [10]. Under the assumption of this separation of time scales, mutations occur only on the evolutionary time scale and not on the ecological time scale.

In the simplest case, a monomorphic population, called the resident, develops along the fast ecological time scale and reaches a steady state, which we call the *resident steady state*. Then, a mutation arises on the slow evolutionary time scale and a mutant phenotype, different from the resident phenotype, emerges. This initially small mutant population interacts with the resident population along the fast ecological time scale. The mutant may die out, or it may grow or invade, depending on the fitness of the mutant phenotype relative to the resident. If the mutant is able to grow, it may replace the resident entirely, causing an evolution in the phenotype. We refer to this phenomenon as *trait substitution*. Alternatively, the two phenotypes may be able to coexist, leading to a dimorphic population with two phenotypes. An invasion of the mutant can also cause both populations to go extinct in a process called *evolutionary suicide* [10]. Based on the assumption that the effect of mutation is small, the mutant phenotype will be similar to the resident phenotype. Hence, adaptive dynamics studies the direction of phenotypic evolution for a given resident type. In the following, we formalize these ideas in terms of mathematical equations and dynamical systems theory.

We begin with the ecological dynamics of a monomorphic resident population, $x$, with phenotype $s_x$, expressed by the deterministic equation

$$\dot{x} = F(x, s_x)x, \tag{1.3.1}$$

where $F$ represents the per-capita growth rate in the population. The dot indicates the derivative with respect to time. On the ecological time scale, this population reaches the resident steady state. The steady state is given by $F(x^*, s_x) = 0$ and will be denoted by $x^* = x^*(s_x)$.

Now a mutation arises on the evolutionary time scale. We introduce a mutant, $y$, with phenotype $s_y$. Since the resident and the mutant interact, we rewrite equation (1.3.1) for the dynamics of the resident as

$$\dot{x} = F(x, s_x; y, s_y)x. \tag{1.3.2}$$

Based on our assumption that the resident and mutant populations differ only in the trait value, the mutant equation is

$$\dot{y} = F(y, s_y; x, s_x)y. \tag{1.3.3}$$

We assume that the initial mutant population is small. We conduct invasion analysis by linearizing the system at the resident steady state $(x, y) = (x^*, 0)$. The equations decouple and we find that the linearization for the mutant is

$$\dot{y} = F(0, s_y; x^*, s_x)y. \tag{1.3.4}$$

The function $F(0, s_y; x^*, s_x) = I(s_x, s_y)$ is known as the mutant's invasion fitness, or as the *invasion exponent* [5, 10]. The mutant can grow if $I > 0$ and will die out if $I < 0$.

We now have a condition for the mutant's ability to invade on the ecological time scale. Under the assumption that invasion implies replacement, this allows us to derive an equation for the trait dynamics on the evolutionary time scale. Following our assumption that mutations are small, we can write $s_y = s_x + \epsilon$ for $|\epsilon| << 1$. Expanding $I(s_x, s_y)$ in a Taylor series with respect to $\epsilon$, we get

$$I(s_x, s_y) = I(s_x, s_x) + \frac{\partial}{\partial_{s_y}} I(s_x, s_x)\epsilon + \frac{\partial^2}{\partial_{s_y^2}} I(s_x, s_x)\frac{\epsilon^2}{2!} + \dots$$

Now $I(s_x, s_x) = F(0, s_x, x^*, s_x) = 0$ by definition, since $(x, y) = (x^*(s_x), 0)$ is a steady state of the adaptive dynamics. Thus, when $\epsilon$ is small, we have

$$I(s_x, s_y) \approx \epsilon \frac{\partial}{\partial s_y} I(s_x, s_y)\Big|_{s_y = s_x}. \tag{1.3.5}$$

The quantity $\partial/\partial s_y I(s_x, s_y)|_{s_y=s_x}$, is called the *selection gradient*. The selection gradient is part of the so-called canonical equation of adaptive dynamics, an ordinary differential equation used to study the evolutionary change of the trait value in a monomorphic population [5, 7]. It is given by

$$\frac{ds_x}{dT} = C \frac{\partial I(s_x, s_y)}{\partial s_y}\Big|_{s_y = s_x}, \tag{1.3.6}$$

where $C > 0$ determines the speed with which the trait changes on the evolutionary time scale, and $T$ denotes evolutionary time.

A *singular point*, which we will denote by $\bar{s}$, is a trait value at which the selection gradient vanishes [10]. We classify such singular points in section 1.3.3.

Trait value pairs, $(s_x, s_y)$, that allow for successful invasion can be visualized in a *pairwise invasibility plot (PIP)*. As an example for finding both the invasion exponent and creating a PIP, we work out an exercise from [10].

### 1.3.2 Example

We consider the Lotka-Volterra competition system for cannibalism. The dynamics of the resident population are described by the equation

$$\dot{x} = xF(x, s_x) = x(r - s_x x + (1 - \epsilon)s_x x), \tag{1.3.7}$$

where $r > 0$ represents the low-density growth rate. The trait value $s_x$ represents the degree of cannibalistic activity in the population. The term $s_x x^2$ represents the loss in the population due to cannibalism and the final term represents the energy gained due to cannabilism, with parameter $0 < \epsilon < 1$ (not to be confused with the use of $\epsilon$ in the preceding section). We study the evolution of trait $s_x$.

The resident equation (1.3.7) has the two steady states

$$x^* = 0, \qquad \text{and} \qquad x^* = \frac{r}{s_x \epsilon} > 0. \tag{1.3.8}$$

The positive steady state is globally stable for all solutions with positive initial condition.

We assume that the resident population has reached this equilibrium, and we introduce a small mutant population, $y$. The resident and mutant equations become

$$\begin{aligned} \dot{x} &= xF(x, s_x, y, s_y) = x(r - s_x x - s_y y + (1-\epsilon)s_x(x+y)) \\ \dot{y} &= yF(y, s_y, x, s_x) = y(r - s_x x - s_y y + (1-\epsilon)s_y(x+y)), \end{aligned} \tag{1.3.9}$$

where the terms $s_y yx$ and $s_x xy$ represent loss in each population due to cannibalism from the other population. When the above system is linearized at the positive steady state $(x, y) = (x^*, 0)$, the mutant equation decouples and becomes

$$\dot{y} = yF(0, s_y, x^*, s_x) = y\left(r - \frac{r}{\epsilon} + (1-\epsilon)\frac{r s_y}{\epsilon s_x}\right). \tag{1.3.10}$$

Thus, the invasion exponent is

$$I(s_x, s_y) = \frac{r(1-\epsilon)(s_y - s_x)}{\epsilon s_x}, \tag{1.3.11}$$

and we have

$$I(s_x, s_y) > 0 \iff s_y > s_x. \tag{1.3.12}$$

Therefore, if $s_y > s_x$, the mutant population is able to grow when introduced into the resident population. Otherwise, the mutant cannot grow.

The corresponding selection gradient is

$$\frac{\partial}{\partial s_y} I(s_x, s_y)\big|_{s_y = s_x} = \frac{(1-\epsilon)r}{\epsilon s_x}. \tag{1.3.13}$$

This selection gradient is always positive, therefore there is no singular point. Furthermore, we have the following lemma.

**Lemma 1.3.1.** *If $s_y > s_x$, then all solutions of (1.3.9) with positive initial conditions converge to the equilibrium $(0, r/\epsilon s_y)$.*

**Proof:** Assume that $s_y > s_x$. We first show that the equilibrum $(0, r/\epsilon s_y)$ is locally stable. The system (1.3.9) has 4 steady states

$$(0,0), \quad \left(\frac{r}{\epsilon s_x}, 0\right), \quad \left(0, \frac{r}{\epsilon s_y}\right), \quad \text{and} \quad \left(-\frac{r}{s_y - s_x}, \frac{r}{s_y - s_x}\right). \tag{1.3.14}$$

The entries of the last steady state have opposite signs. Thus, this state is not biologically relevant.

We evaluate the local stability of each viable steady state in the traditional manner by looking at the Jacobian matrix [30]. For the first steady state, $(0,0)$, the associated Jacobian matrix has repeated eigenvalue, $r > 0$. Thus, it is unstable. This condition is independent of any relation between the two trait values.

For the 2nd steady state, $(r/\epsilon s_x, 0)$, the associated Jacobian matrix has eigenvalues

$$\frac{r(1-\epsilon)(s_y - s_x)}{\epsilon s_x} \qquad \text{and} \qquad -r < 0. \tag{1.3.15}$$

The first eigenvalue is greater than zero when $s_y > s_x$, making this state unstable.

For the 3rd steady state, $(0, r/\epsilon s_y)$, the Jacobian matrix has eigenvalues

$$-r < 0 \qquad \text{and} \qquad \frac{-r(1-\epsilon)(s_y - s_x)}{\epsilon s_y}. \tag{1.3.16}$$

Both eigenvalues are negative when $s_y > s_x$, indicating that this state is locally stable.

We now show that $(0, r/\epsilon s_y)$ is also globally stable. We first rule out the existence of periodic orbits in the positive quadrant, using Dulac's criterion [34]. We apply the method in example 7.2.4 of [34].

Letting $X = (x, y)$, we choose $g(X) = 1/xy$ with $x, y > 0$. This function, $g$, is continuously differentiable and real-valued as required. We have

$$\begin{aligned}
\nabla \cdot (g\dot{X}) &= \frac{\partial}{\partial x}(g\dot{x}) + \frac{\partial}{\partial y}(g\dot{y}) \\
&= \frac{\partial}{\partial x}\left(\frac{r - s_x x - s_y y + (1-\epsilon)s_x(x+y)}{y}\right) \\
&+ \frac{\partial}{\partial y}\left(\frac{r - s_x x - s_y y + (1-\epsilon)s_y(x+y)}{x}\right) \\
&= \frac{1}{y}(-s_x + (1-\epsilon)s_x) + \frac{1}{x}(-s_y + (1-\epsilon)s_y) \\
&= -\epsilon\left(\frac{s_x}{y} + \frac{s_y}{x}\right) \\
&< 0.
\end{aligned} \tag{1.3.17}$$

Thus, $\nabla \cdot (g\dot{X}) < 0$ has one sign throughout the positive quadrant. Since the vector field in (1.3.9) is continuously differentiable in the simply connected region $x, y > 0$, there can be no periodic orbits in the positive quadrant.

We now show that every trajectory in the positive quadrant remains bounded.

We pick $\bar{x} > x^* = r/\epsilon s_x$. Then if $(x(t), y(t))$ is a solution with $x(t) > \bar{x}$, we have

$$\begin{aligned} \dot{x} &= x(r - s_x x - s_y y + (1-\epsilon)s_x(x+y)) \\ &< r + (s_x - s_y)y - \epsilon s_x y - \epsilon s_x x \\ &< r - \epsilon s_x x \\ &< 0. \end{aligned} \tag{1.3.18}$$

Hence, all solutions eventually have $x(t) \leqslant \bar{x}$.We now set

$$\bar{y} = \frac{r + (s_y - s_x)\bar{x}}{\epsilon s_y}. \tag{1.3.19}$$

Then, for a solution with $y(t) > \bar{y}$, we have

$$\begin{aligned} &\epsilon r - s_x x + s_y x - \epsilon s_y y < 0 \\ &\implies r - s_x x + (1-\epsilon)s_y x - \epsilon s_y y - s_y y + s_y y < 0 \\ &\implies r - s_x x - s_y y + (1-\epsilon)s_y(x+y) < 0 \\ &\implies \dot{y} < 0 \end{aligned} \tag{1.3.20}$$

Hence, all solutions eventually have $y(t) \leqslant \bar{y}$. Thus, all trajectories are bounded and the region $R = [0, \bar{x}] \times [0, \bar{y}]$ is an attracting set. Therefore, we can apply the *Poincaré-Bendixson* theorem [32]. Since all trajectories are bounded within $R$, and there can be no periodic orbits, the $\omega$-limit set of (1.3.9) contains at least one stationary point.

We showed that the steady state $(x^*, y^*) = (0, 0)$ is a source, and thus it cannot be part of the $\omega$-limit set. Alternatively, the saddle point, $(x^*, y^*) = (r/\epsilon s_x, 0)$ could be part of a homoclinic orbit. However, since the stable manifold comes from the source at $(0, 0)$, we can also rule out this possibility. Therefore, all trajectories go towards the locally stable steady state, $(0, r/\epsilon s_y)$.

Therefore the steady state $(0, r/\epsilon s_y)$ is globally stable. ∎

In figure 1.1, we have created a pairwise invasibility plot (PIP) for this example. The shaded region represents trait values such that $I(s_x, s_y) > 0$ while the unshaded region represents values where $I(s_x, s_y) < 0$.

### 1.3.3 Classification of singular points

In example 1.3.2, we illustrated a very simple case for adaptive dynamics where the selection gradient did not have a singular point. In reality, the evolutionary dynamics can be much more complicated. In this section, we will detail how to classify the behaviour of a system near its singular points and give an example of a system where a singular point is present.

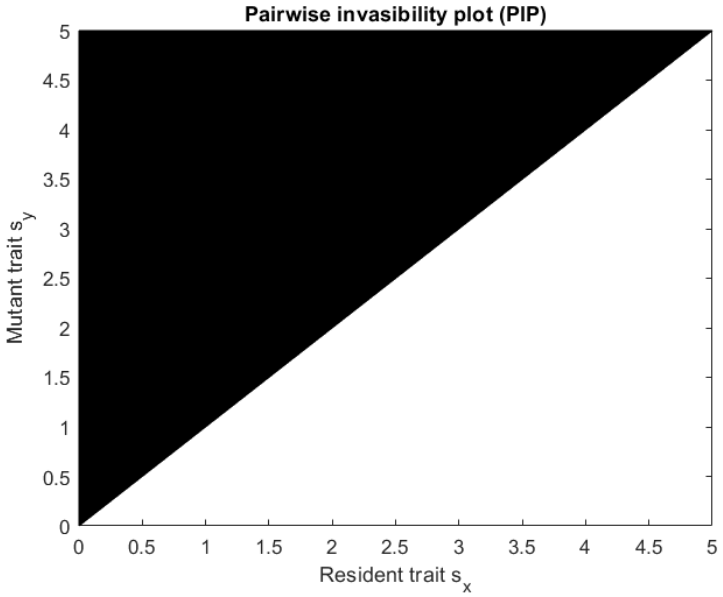


Figure 1.1: Pairwise invasibility plot (PIP) for the cannibalism example with invasion exponent (1.3.11). By lemma 1.3.1, the invader replaces the resident for trait value pairs in the shaded region.

From the definition of the invasion exponent, we have that $I(s_x, s_x) = 0$. Using this identity, we also get

$$\begin{aligned} \frac{\partial I}{\partial s_x}\Big|_{s_y=s_x} + \frac{\partial I}{\partial s_y}\Big|_{s_y=s_x} &= 0, \\ \frac{\partial^2 I}{\partial s_x^2}\Big|_{s_y=s_x} + 2\frac{\partial^2 I}{\partial s_x \partial s_y}\Big|_{s_y=s_x} + \frac{\partial^2 I}{\partial s_y^2}\Big|_{s_y=s_x} &= 0. \end{aligned} \tag{1.3.21}$$

To simplify notation, we define

$$c_{11} = \frac{\partial^2 I}{\partial s_x^2}\Big|_{s_y=s_x}, \quad c_{22} = \frac{\partial^2 I}{\partial s_y^2}\Big|_{s_y=s_x}, \quad c_{12} = \frac{\partial^2 I}{\partial s_x \partial s_y}\Big|_{s_y=s_x} = -\frac{1}{2}(c_{11} + c_{22}), \tag{1.3.22}$$

where the simplification of $c_{12}$ comes from (1.3.21).

We use these derivatives to classify singular points by looking at four different possibilities [10, 18].

**Possibility 1**: If $\bar{s}$ is a singular point that cannot be invaded by nearby strategies, then $\bar{s}$ is called an *evolutionary stable strategy (ESS)*. Nearby strategies cannot succeed if the invasion exponent is negative. Hence, we require $I(\bar{s}, s_y)$ to have a local maximum in $s_y = \bar{s}$. Thus, a singular point is an ESS if $c_{22} < 0$. Geometrically, this means that a vertical line drawn through the singular point of the PIP will lie (locally) in the region where $I < 0$.

**Possibility 2**: If successful strategies are nearer to $\bar{s}$ than the resident, then $\bar{s}$ is a local attractor for the adaptive dyamics and is called a *convergence stable strategy (CSS)*. Alternatively, if successful strategies are farther from $\bar{s}$, the singular point is a repeller for the adaptive dynamics. If successful strategies are nearer to $\bar{s}$, then the selection gradient is positive for $s_x < \bar{s}$ and negative for $\bar{s} < s_x$. Hence, at $s_x = \bar{s}$, the second derivative of the selection gradient must be negative, such that

$$0 > \left[\frac{\partial}{\partial s_x}\left(\frac{\partial}{\partial s_y} I(s_x, s_y)\Big|_{s_y=s_x}\right)\right]\Big|_{s_x=\bar{s}} = c_{12} + c_{22}\Big|_{s_y=s_x=\bar{s}} = \frac{1}{2}(c_{22} - c_{11})\Big|_{s_y=s_x=\bar{s}} \tag{1.3.23}$$

Therefore $\bar{s}$ is convergent stable if $c_{11} > c_{22}$ at $s_y = s_x = \bar{s}$. Geometrically, if $I > 0$ above the diagonal on the left and below the diagonal on the right of $\bar{s}$ then $\bar{s}$ is convergent stable [18]. Convergent stable strategies are called *evolutionary attractors* [26]. A singular point that is both an ESS and convergent stable is called a *continuously stable strategy* [13, 14].

**Possibility 3**: If the singular strategy can invade a nearby resident, the invasion exponent must be positive, so $I(s_x, \bar{s})$ needs to have a local minumum at $s_x = \bar{s}$. Thus, we have the criteria $c_{11} > 0$ at $s_x = \bar{s}$. Geometrically, this means that a horizontal line through $\bar{s}$ lies locally in the region where $I > 0$.

**Possibility 4**: We speak of *mutual invasibility* if $I(s_x, s_y) > 0$ and $I(s_y, s_x) > 0$. This occurs when $I(s_x, 2\bar{s} - s_x)$ has a local minimum at $s_x = \bar{s}$. The first derivative of $I$ in this case is

$$\frac{\partial I}{\partial s_x} - \frac{\partial I}{\partial s_y}, \tag{1.3.24}$$

which has second derivative $c_{11} - 2c_{12} + c_{22} = 2c_{11} + 2c_{22}$. Thus, mutual invasibility occurs when $c_{11} > -c_{22}$. Geometrically, this means that the line $s_y = 2\bar{s} - s_x$ lies locally in the region where $I > 0$.

Mutual invasibility may lead to the coexistence of two subpopulations with different traits. This scenario, sometimes called *branching*, changes our monomorphic population into a dimorphic population. In order to analyze such dynamics, different methods must be used, which we will not detail in this thesis. In the following section, we generalize the previous example and apply the classification for singular points.

### 1.3.4 Example for classification of singular points

We introduce a tradeoff into example 1.3.2. This idea is novel and not previously introduced in [10]. We suppose that as individuals improve their ability to cannibalize, their efficiency at producing offspring decreases. To represent this tradeoff, we replace the growth rate $r$ with a positive decreasing function $r(s)$. The resident ODE for the monomorphic population becomes

$$\dot{x} = xF(x, s_x) = x\left(r(s_x) - \epsilon s_x x\right), \tag{1.3.25}$$

which has the two steady states

$$x^* = 0, \qquad \text{and} \qquad x^* = \frac{r(s_x)}{\epsilon s_x} > 0. \tag{1.3.26}$$

As in the previous example, we assume that the resident reaches the positive steady state and introduce the mutant population $y$. We get the system

$$\begin{aligned} \dot{x} &= xF(x, y, s_x, s_y) = x(r(s_x) - s_x x - s_y y + (1-\epsilon)s_x(x+y)), \\ \dot{y} &= yF(y, x, s_y, s_x) = y(r(s_y) - s_x x - s_y y + (1-\epsilon)s_y(x+y)). \end{aligned} \tag{1.3.27}$$

Linearizing the above system at the steady state $(x, y) = (x^*, 0)$, the mutant equation decouples and becomes

$$\dot{y} = yF(0, x^*, s_y, s_x) = y\left(r(s_y) - \frac{r(s_x)}{\epsilon} + \frac{(1-\epsilon)r(s_x)s_y}{\epsilon s_x}\right). \tag{1.3.28}$$

Hence, the invasion exponent is

$$I(s_x, s_y) = r(s_y) + \frac{r(s_x)((1-\epsilon)s_y - s_x)}{\epsilon s_x}, \tag{1.3.29}$$

which has first order partial derivatives

$$\begin{aligned} \frac{\partial I}{\partial s_x} &= \frac{r'(s_x)((1-\epsilon)s_y - s_x)}{\epsilon s_x} - \frac{r(s_x)(1-\epsilon)s_y}{\epsilon s_x^2}, \\ \frac{\partial I}{\partial s_y} &= r'(s_y) + \frac{(1-\epsilon)r(s_x)}{\epsilon s_x}, \end{aligned} \tag{1.3.30}$$

and second order partial derivatives

$$\begin{aligned} \frac{\partial^2 I}{\partial s_x^2} &= \frac{r''(s_x)((1-\epsilon)s_y - s_x)}{\epsilon s_x} - \frac{2(1-\epsilon)s_y(r'(s_x)s_x - r(s_x))}{\epsilon s_x^3}, \\ \frac{\partial^2 I}{\partial s_y^2} &= r''(s_y), \\ \frac{\partial^2 I}{\partial s_x \partial s_y} &= \frac{(1-\epsilon)(r'(s_x)s_x - r(s_x))}{\epsilon s_x^2}. \end{aligned} \tag{1.3.31}$$

The corresponding selection gradient is

$$\frac{\partial}{\partial s_y} I(s_x, s_y)\Big|_{s_y = s_x} = r'(s_x) + \frac{(1-\epsilon)r(s_x)}{\epsilon s_x}. \tag{1.3.32}$$

Now suppose we have some singular point $\bar{s}$. We check the conditions for each possibility outlined in the previous section using the derivatives in (1.3.31). Firstly,

$\bar{s}$ is an ESS if $r''(\bar{s}) < 0$. Secondly, $\bar{s}$ is a CSS and an attractor for the adaptive dynamics if $c_{11} > c_{22}$, or

$$r''(\bar{s}) + \frac{1-\epsilon}{\epsilon\bar{s}} r'(\bar{s}) - \frac{1-\epsilon}{\epsilon\bar{s}^2} r(\bar{s}) < 0, \tag{1.3.33}$$

and a repeller if $c_{11} < c_{22}$.

Thirdly, we suppose that the mutant has strategy $\bar{s}$ and the resident has some nearby strategy. The mutant can successfully invade if $c_{11} > 0$ at $s_x = \bar{s}$, i.e. if

$$r''(\bar{s}) + \frac{2(1-\epsilon)}{\epsilon\bar{s}} r'(\bar{s}) - \frac{2(1-\epsilon)}{\epsilon\bar{s}^2} r(\bar{s}) < 0. \tag{1.3.34}$$

Lastly, we have mutual invasibility if $I(s_x, s_y) > 0$ and $I(s_y, s_x) > 0$ which occurs when $c_{11} > -c_{22}$, such that

$$r'(\bar{s}) - \frac{r(\bar{s})}{\bar{s}} < 0. \tag{1.3.35}$$

For more concrete results, the function $r(s_x)$ must be specified. We choose $r(s_x) = \bar{r}e^{-as_x}$, where $\bar{r} > 0$ is the growth rate in the absence of cannibalism and $a > 0$ is a parameter. As required, $r(s_x)$ is a positive decreasing function of the trait value. The selection gradient in (1.3.32) is now

$$\frac{\partial}{\partial s_y} I(s_x, s_y)\Big|_{s_y = s_x} = \bar{r}e^{-as_x}\left(-a + \frac{1-\epsilon}{\epsilon s_x}\right). \tag{1.3.36}$$

The singular point for this selection gradient is

$$\bar{s} = \frac{1-\epsilon}{a\epsilon}. \tag{1.3.37}$$

This point cannot be an ESS since $r''(s_x) = a^2 r(s_x) > 0$. The singular point will be a CSS and an attractor for the adaptive dynamics if it satisfies

$$a^2 - \frac{1-\epsilon}{\epsilon\bar{s}} a - \frac{1-\epsilon}{\epsilon\bar{s}^2} < 0, \tag{1.3.38}$$

or a repeller for the adaptive dynamics if the opposite inequality holds. For the singular point in equation (1.3.37), the above inequality simplifies to

$$\frac{\epsilon a^2}{1-\epsilon} > 0. \tag{1.3.39}$$

Hence, since $0 < \epsilon < 1$, this singular point is an attractor for the adaptive dynamcis. For our third possibility, the singular strategy can invade a nearby resident if $\bar{s}$ satisfies

$$\bar{s}^2 - \frac{2(1-\epsilon)}{\epsilon a}\bar{s} - \frac{2(1-\epsilon)}{\epsilon a^2} < 0. \tag{1.3.40}$$

This condition simplifies to $\epsilon > -1$, which is always true. Finally, we have mutual invasibility if a singular point $\bar{s}$ satisfies

$$\bar{s} > -\frac{1}{a}, \tag{1.3.41}$$

which is always satisfied since $a > 0$ and $\bar{s} > 0$.

For this example the singular point is not an ESS but it is a CSS for the adaptive dynamics. Additionally, the singular phenotype is able to invade nearby phenotypes and pairs of neighboring phenotypes are able to invade each other. In figure 1.2, trait values for which $I(s_x, s_y) > 0$ are presented in a pairwise invasibility plot (PIP). The singular strategy, $\bar{s}$, is at the intersection of the two shaded regions.

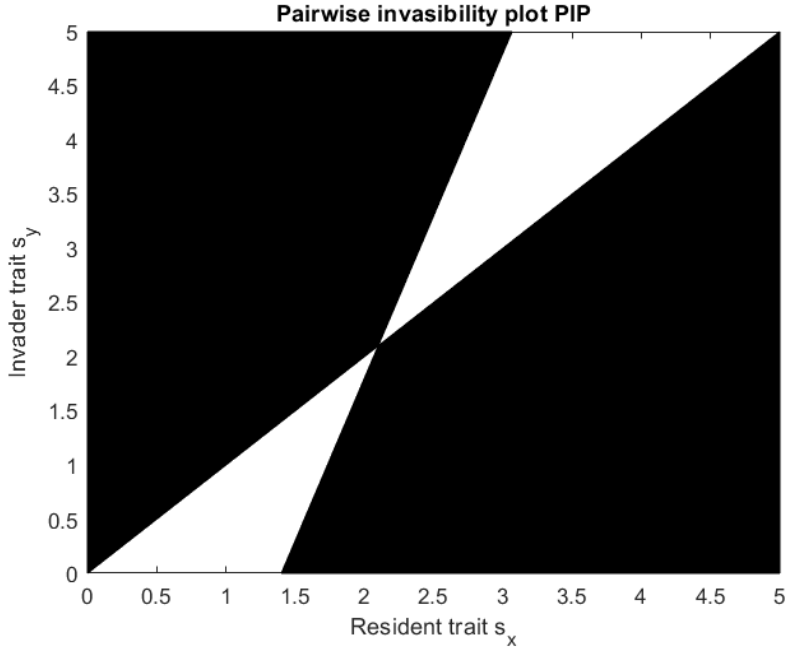


Figure 1.2: Pairwise invasibility plot (PIP) for the revised cannibalism example 1.3.4. The invader successfully invades the resident population for trait values in the shaded region.

## 1.4 Hybrid Models

So far all theory and examples have been applied to population dynamics modelled using continuous differential equations. However, our goal is to create a model for perennial plants in a seasonal environment. In particular, perennials recruit only once a year at the beginning of their growing season but undergo various other dynamics

continuously throughout the season. Although there are various ways to model this environment, we chose to use hybrid models (or impulsive models).

In the simplest case, hybrid models can be used to describe the continuous interactions between a population and its environment throughout the year, along with the discrete reproduction event of the population [31]. Often, using a purely discrete or purely continuous time model cannot accurately describe population growth. For instance, a continuous-time model assumes both mortality and recruitment occur instantaneously. However, for some populations there is a recruitment period that is mainly discrete while other ecological dynamics are continuous during this period. Alternatively, mortality occurs throughout the lifespan, and is thus mostly continuous [17, 20].

For a population of perennial plants, population growth is most easily measured by comparing the number of plants from one year to the next. Recruitment of new plants occurs only during a certain part of the year and is best measured in discrete time jumps. However, plant growth, mortality, and pollination all occur continuously throughout the growing season. These two different time scales make a hybrid model useful to represent the full population dynamic.

We now present an example of a very simple hybrid model that can be solved explicitly and reduced to a discrete-time model. The goal is to calculate the steady state(s) of the model and evaluate stability. In example 1.3.2, we performed these calculations for a continuous model. For a hybrid model the method differs slightly. We detail the steps to obtain the steady state below.

We consider a plant that emerges and grows during a certain period of the year after which it remains dormant until the following year. We track the biomass of the plant from year to year in discrete time. The biomass of the plant at the end of year $T$ will be denoted by $x(T)$. The plant then survives through the winter with probability $0 < \gamma < 1$, and emerges at the beginning of the following year, $T + 1$, with biomass $\gamma x(T)$.

During the season, the plant biomass grows according to the standard logistic differential equation

$$f'(t) = rf(t)\left(1 - \frac{f(t)}{K}\right), \qquad 0 < t < t_1, \tag{1.4.1}$$

where $r \geqslant 0$ is the rate of maximum biomass growth, $K > 0$ is the carrying capacity of the environment, and $t_1$ represents the length of the growing season. The initial condition for the equation is the plant biomass at the beginning of the season, $f(0) = \gamma x(T)$. The solution to (1.4.1) is

$$f(t) = \frac{K\gamma x(T)e^{rt}}{K + \gamma x(T)(e^{rt} - 1)}. \tag{1.4.2}$$

The biomass at the end of the season is $x(T+1) = f(t_1)$. Hence, the discrete recursion equation to update the plant population each year is

$$x(T+1) = \frac{K\gamma x(T)e^{rt_1}}{K + \gamma x(T)(e^{rt_1} - 1)}. \tag{1.4.3}$$

The recursion equation has two steady states

$$x^* = 0, \qquad \text{and} \qquad x^* = \frac{K(\gamma e^{rt_1} - 1)}{\gamma(e^{rt_1} - 1)}. \tag{1.4.4}$$

The second steady state is only positive when $\gamma e^{rt_1} > 1$. We analyze the stability of the two steady states by evaluating the linearization of (1.4.3) at each steady state. We find that the zero steady state is stable only if $\gamma e^{rt_1} < 1$ and the non zero steady state is stable only if $\gamma e^{rt_1} > 1$. Thus, whenever the positive steady state is present in the system, it is stable. Otherwise the plant population tends to zero. Hence, at the point $\gamma e^{rt_1} = 1$, the system has a transcritical bifurcation. This is illustrated numerically with a cobweb diagram in figure 1.3.

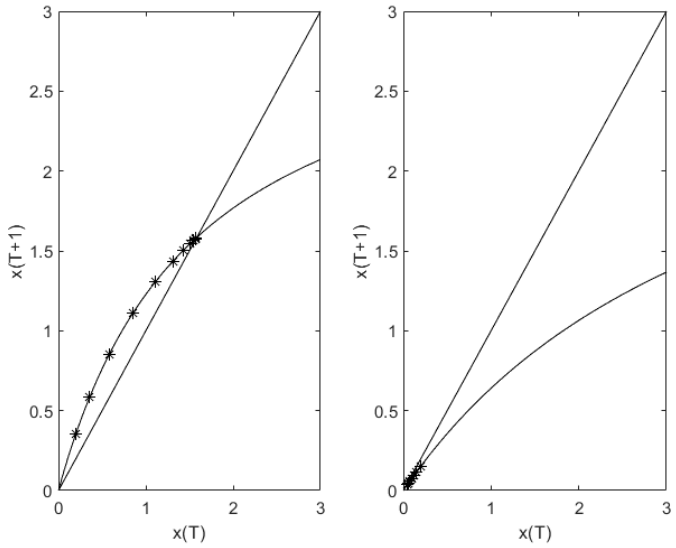


Figure 1.3: Cobweb for the hybrid model (1.4.3) when the positive steady state exists (left), and when only the zero steady state exists (right).

This example describes a perennial plant with very simple dynamics. The model equation appears in various places in the literature. The model does not include flowering and reproduction but instead models only the vegetative growth of the plant. In the next chapter we derive our model for a perennial plant, which includes more complicated evolutionary and ecological dynamics.

## 1.5 Thesis outline

In chapter 2, we derive a model for the evolution of flowering onset in a perennial plant. We then nondimensionalize the model (section 2.2) in order to reduce the number of parameters. We prove that the zero state of our model is locally stable, and we discuss the biological consequences of this result (section 2.3). We present brief numerical results for the nondimensionalized model (section 2.4) for one special case. However, the full model is too complex to allow for in-depth analysis. Instead, we consider two simplifications that can be analyzed to some extent, and compare the results.

In chapter 3, we apply the adaptive dynamics framework to our model. We present and prove several properties of the resident-only model (section 3.1). We then introduce the mutant population and perform invasion analysis (section 3.2).

In chapter 4, we reduce our model to a model for the mean trait value and population density. We present the derivation of the required moment equations (section 4.1), and apply a particular distribution to the derived model (section 4.2). We simulate the model and present the results in section 4.3.

In chapter 5, we close the thesis with a discussion of our work and some suggestions for future directions.

# Chapter 2

# Model derivation and basic properties

## 2.1 Model derivation

In this chapter, we derive our novel model for the evolution of flowering time in a perennial plant. We are not aware of any other attempt in the literature to model the evolution of flowering time with a similar approach. Our trait of interest is the time after emergence that flowering begins. This trait will be denoted by $s$. The total population of perennial plants may change from year to year, but each individual plant has a growth and dormant period within the year. To capture this behaviour the model is separated into two time scales. The year, denoted by $T$, will be represented in discrete time, and days within the year, denoted by $t$, will be represented in continuous time.

The plant emerges and begins to grow at time $t = t_0$. We assume that the growth and flowering phase of the plant occur separately [33]. The plant grows until it flowers, i.e. for $t \in [t_0, t_0 + s]$. Flowering lasts until the season ends at time $t = t_1$. The length of the season will be denoted $t_g = t_1 - t_0$. These dynamics are illustrated in figure 2.1. In table 2.1 we present the variables and parameters that will be used in the model.

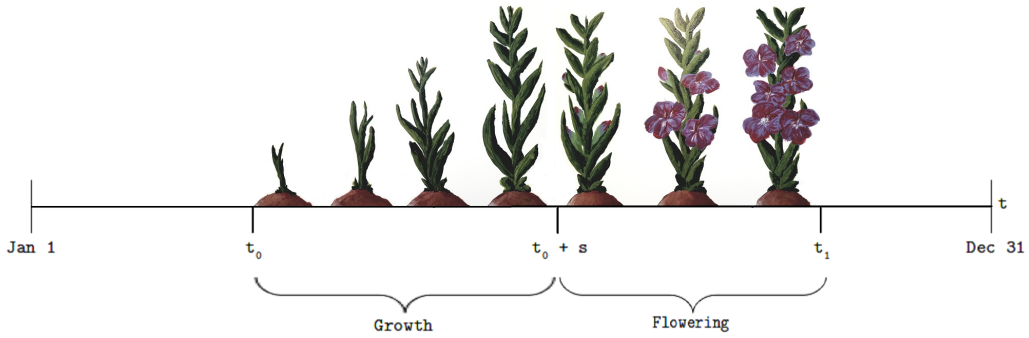


Figure 2.1: Illustration of the timeline for our model.

Table 2.1: Table of Model Quantities

| Quantity | Representation |
|---|---|
| $s$ | Flowering time trait value, measured in days since emergence |
| $t$ | Time within the year, measured in days |
| $T$ | Time, measured in years |
| $N(T;s)$ | Plant population with trait $s$ at the beginning of year $T$ |
| $F(t;s)$ | Unpollinated flowers with trait $s$ at time $t$ |
| $\hat{S}(t)$ | Total density of seeds produced |
| $\hat{S}(t_1;s)$ | Density of seeds with trait $s$ at time $t=t_1$ |
| $S(T;s)$ | Seed population with trait $s$ at the end of year $T$ |
| $t_0$ | Beginning of the plant growing season |
| $t_1$ | End of the plant growing season |
| $t_g$ | Length of the season |
| $\nu$ | Rate of conversion of biomass into flowers |
| $\mu$ | Natural death rate of flowers |
| $\rho$ | Rate of pollination between flowers |
| $\alpha$ | Strength of density-dependence among seedlings |
| $m$ | Heritability proportion |
| $\sigma_K^2$ | Variance of the mutation kernel |
| $\gamma$ | Probability of successful plant overwintering |
| $\omega$ | Probability of successful seed germination |
| $\xi$ | Number of seeds produced per pollinated flower |

The number of plants with flowering time $s$ in year $T$ will be denoted by $N(T;s)$. To update the plant population from year to year, we use the recursion equation

$$N(T+1;s) = \gamma N(T;s) + \omega S(T;s), \tag{2.1.1}$$

where $\gamma$ is the probability of successful overwintering of plants from the previous year, $S(T;s)$ the population of seeds produced during the previous year, and $\omega$ the probability of successful germination.

In order to determine the number of seeds with flowering time $s$ that will be produced by the end of the year, we model growth, pollination, and seed production during the season. To begin, plants grow according to some function $g(t)$. The biomass of a plant with flowering time $s$ will be denoted by $B(t;s)$ and represented by the equation

$$\frac{\partial}{\partial t}B(t;s) = g(t), \tag{2.1.2}$$

where $t_0 < t < t_0 + s$, and $B(t_0;s) = 0\ \forall s$. In the simplest case, wherein $g(t) = g$ is some constant growth rate, we have

$$B(t_0+s;s) = \int_{t_0}^{t_0+s} g(t)dt = gs. \tag{2.1.3}$$

The population of unpollinated flowers will be denoted by $F(t;s)$ and represented by the equation

$$\frac{\partial}{\partial t}F(t;s) = \frac{\nu B(t_0+s;s)N(T;s)}{1+\alpha\int_0^{t_g} N(T;s')ds'} - \mu F(t;s) - \rho F(t;s)\int_0^{t_g} F(t;s')ds', \tag{2.1.4}$$

where the first term represents floral growth, the second term the natural mortality of flowers, and the third term the pollination of a flower with trait $s$ by a flower of any other trait, $s'$. Since flowers with trait $s$ begin growing at time $t_0+s$, this equation has initial condition $F(t_0+s;s) = 0$, and $F(t;s)$ is defined for $t \in (t_0+s, t_1)$. This makes the equation difficult to analyze because the pollination term requires integration over all possible trait values, for $s'$ from 0 to $t_g = t_1 - t_0$. To deal with this issue, we introduce the Heaviside function, $\mathcal{H}(t-s)$, which is defined as

$$\mathcal{H}(t-s) = \begin{cases} 1, & t > s, \\ 0, & t < s. \end{cases} \tag{2.1.5}$$

With this notation, we can write (2.1.4) as

$$\frac{\partial}{\partial t}F(t;s) = \frac{\nu B(t_0+s;s)\mathcal{H}(t-s)N(T;s)}{1+\alpha\int_0^{t_g} N(T;s')ds'} - \mu F(t;s) - \rho F(t;s)\int_0^{t_g} F(t;s')ds', \tag{2.1.6}$$

for $t_0 < t < t_1$ and initial condition $F(t_0; s) = 0\ \forall s$.

According to (2.1.6), the rate of pollination for flowers with trait $s_1$, by flowers with trait $s_2$, is given by $\rho F(t; s_1)F(t; s_2)$. The total density of all seeds produced by pollination is denoted by $\hat{S}(t)$. We assume that each flower produces an equal number of viable seeds, so that the density of pollinated flowers is proportional to the density of seeds produced. We denote this proportionality constant by $\xi$. The rate of change for $\hat{S}(t)$ is therefore given by

$$\frac{d}{dt}\hat{S}(t) = \xi\rho \int_0^{t_g} \int_0^{t_g} F(t; s_1)F(t; s_2)ds_1 ds_2. \tag{2.1.7}$$

The density of seeds with trait $s$ at time $t$ is denoted by $\hat{S}(t; s)$. To determine the flowering time of a particular seed, assumptions must be made regarding heritability. If the seed solely inherits the trait of the"mother" (or "father") plant, then the rate of change of seeds with flowering time $s$ is given by

$$\frac{\partial}{\partial t}\hat{S}(t; s) = \xi\rho F(t; s) \int_0^{t_g} F(t; s_1)ds_1 \tag{2.1.8}$$

This special case, called *clonal reproduction*, will be studied in chapter 3. Instead, we can assume that the flowering time, $s$, of the seed is given by some convex combination of its parental traits, $s_1$ and $s_2$. We express this assumption as

$$ms_1 + (1 - m)s_2 = s, \qquad 0 < m < 1. \tag{2.1.9}$$

Solving (2.1.9) for $s_2$, we make a change of variables $s_2 = (s - ms_1)/(1 - m)$ in (2.1.7) to find

$$\frac{d}{dt}\hat{S}(t) = \xi\rho \int_0^{t_g} \int_{ms_1}^{ms_1+(1-m)t_g} F(t; s_1)F\left(t; \frac{s - ms_1}{1 - m}\right) \frac{ds}{1 - m} ds_1. \tag{2.1.10}$$

To simplify these expressions slightly we define $F(\cdot; s)$ to be a function on all of $\mathbb{R}$ by setting $F(\cdot; s) = 0$ for all $s \notin [0, t_g]$. Then the integrals involved can be taken over the entire real line.

The density of seeds with flowering time $s$ at the end of the season is obtained as

$$\hat{S}(t_1; s) = \xi\rho \int_{t_0}^{t_1} \left( \int_{-\infty}^{\infty} F(t; s_1)F\left(t; \frac{s - ms_1}{1 - m}\right) \frac{ds_1}{1 - m} \right) dt. \tag{2.1.11}$$

In this notation, the total density of seeds at the end of the season is $\hat{S}(t_1) = \int \hat{S}(t_1; s)ds$.

Finally we introduce the possibility of mutation into our model. We denote by $K(s - s')$ the probability that a plant from a seed with flowering time $s'$ will flower

at time $s$. Then the total number of seeds with flowering time $s$ in year $T$ is denoted by $S(T;s)$ and given by

$$S(T;s) = \int_{-\infty}^{\infty} K(s-s')\hat{S}(t_1;s')ds', \tag{2.1.12}$$

where $K$ is some suitable probability distribution. The effects of mutation are not the focus of this thesis, and hence, we will make the simplest possible assumption that $K$ is a unimodal symmetric distribution with mean zero. When required, the variance of the distribution will be denoted by $\sigma_K^2$.

Under these assumptions, equation (2.1.1) becomes

$$N(T+1;s) = \gamma N(T;s) + \omega\xi\rho \int_{t_0}^{t_1}\int_{-\infty}^{\infty}\int_{-\infty}^{\infty} K(s-s')F(t;s_1)F\left(t;\frac{s'-ms_1}{1-m}\right)\frac{ds_1}{1-m}ds'dt, \tag{2.1.13}$$

where the flowers, $F$, are found by solving (2.1.6).

## 2.2 Nondimensionalization of the model

We nondimensionalize our system in order to simplify the model and reduce the number of parameters.

We begin by writing $n = N/\hat{N}$, $f = F/\hat{F}$, $\tau = t/\hat{t}$, and $\sigma = s/\hat{t}$, where $\hat{N}$, $\hat{F}$, and $\hat{t}$ have the required units and $n$, $f$, $\tau$, and $\sigma$ are dimensionless. We nondimensionalize only for the case where biomass growth is constant, as in (2.1.3). Applying the change of variables to (2.1.6), we get

$$\begin{aligned}\frac{\partial f}{\partial \tau} &= \frac{\hat{t}}{\hat{F}}\frac{\partial F}{\partial t} \\ &= \frac{\hat{t}}{\hat{F}}\frac{\nu g\hat{t}\sigma\mathcal{H}(\hat{t}(\tau-\sigma))\hat{N}n(T;\hat{t}\sigma)}{1+\alpha\hat{t}\hat{N}\int_{-\infty}^{\infty}n(T;\hat{t}\sigma')d\sigma'} - \mu\hat{t}f - \rho\hat{t}^2\hat{F}f\int_{-\infty}^{\infty}f(\hat{t}\tau;\hat{t}\sigma')d\sigma'.\end{aligned} \tag{2.2.1}$$

A straight forward choice would be to set $\mu = 1/\hat{t}$. However, after multiple numerical simulations, we found that the system was most sensitive to changes in the death rate, $\mu$. Hence, we chose a nondimensionalization that keeps $\mu$ as the primary parameter in the model. Therefore, we set $\rho\hat{t}^2\hat{F} = 1$, $\nu g\hat{t}\hat{N}/\hat{F} = 1$, and $\alpha\hat{t}\hat{N} = 1$. Solving the three equations, we find that we must choose

$$\hat{t} = \left(\frac{\alpha}{\rho\nu g}\right)^{1/3}, \qquad \hat{F} = \left(\frac{\nu g}{\alpha\sqrt{\rho}}\right)^{2/3}, \qquad \hat{N} = \left(\frac{\rho\nu g}{\alpha^4}\right)^{2/3}. \tag{2.2.2}$$

Hence, we have

$$\frac{\partial f}{\partial \tau} = \frac{\sigma\mathcal{H}(\tau-\sigma)n(T;\hat{t}\sigma)}{1+\int_{-\infty}^{\infty}n(T;\hat{t}\sigma')d\sigma'} - f(\hat{t}\tau;\hat{t}\sigma)\left(\hat{\mu}+\int_{-\infty}^{\infty}f(\hat{t}\tau;\hat{t}\sigma')\sigma'\right), \tag{2.2.3}$$

where

$$\hat{\mu} = \mu \left( \frac{\alpha}{\rho \nu g} \right)^{1/3}. \tag{2.2.4}$$

Applying the change of variables to (2.1.13), we get

$$\begin{aligned} n(T+1;\hat{t}\sigma) &= \gamma n(T;\hat{t}\sigma) \\ &+ \frac{\omega \xi \rho \tilde{F}^2 \hat{t}^2}{\tilde{N}} \int_{t_0/\hat{t}}^{t_1/\hat{t}} \int_{-\infty}^{\infty} \int_{-\infty}^{\infty} \hat{t} K(\hat{t}(\sigma - \sigma')) f(\hat{t}\tau; \hat{t}\sigma_1) f\left( \hat{t}\tau; \hat{t} \frac{\sigma' - m\sigma_1}{1-m} \right) \frac{d\sigma_1}{1-m} d\sigma' d\tau. \end{aligned} \tag{2.2.5}$$

Setting

$$\hat{\omega} = \omega \xi \left( \frac{\nu g \alpha^2}{\rho^2} \right)^{1/3}, \qquad \hat{t_1} = t_1 \left( \frac{\rho \nu g}{\alpha} \right)^{1/3}, \qquad \hat{t_0} = t_0 \left( \frac{\rho \nu g}{\alpha} \right)^{1/3}, \tag{2.2.6}$$

we get

$$\begin{aligned} n(T+1;\hat{t}\sigma) &= \gamma n(T;\hat{t}\sigma) \\ &+ \hat{\omega} \int_{\hat{t_0}}^{\hat{t_1}} \int_{-\infty}^{\infty} \int_{-\infty}^{\infty} \hat{K}(\sigma - \sigma') f(\hat{t}\tau; \hat{t}\sigma) f\left( \hat{t}\tau; \hat{t} \frac{\sigma' - m\sigma_1}{1-m} \right) \frac{d\sigma_1}{1-m} d\sigma' d\tau, \end{aligned} \tag{2.2.7}$$

where $\hat{K}(\sigma - \sigma') = \hat{t} K(\hat{t}(\sigma - \sigma'))$. The mean of $\hat{K}(y)$ is zero and the variance is

$$\sigma_{\hat{K}}^2 = \left( \frac{\alpha}{\rho \nu g} \right)^{2/3} \sigma_K^2. \tag{2.2.8}$$

To simplify notation, we write $\hat{n}(T;\sigma) = n(T;\hat{t}\sigma)$ and $\hat{f}(\tau;\sigma) = f(\hat{t}\tau;\hat{t}\sigma)$. Thus, the general model in nondimensionalized form is

$$\begin{aligned} \hat{n}(T+1;\sigma) &= \gamma \hat{n}(T;\sigma) \\ &+ \hat{\omega} \int_{\hat{t_0}}^{\hat{t_1}} \int_{-\infty}^{\infty} \int_{-\infty}^{\infty} \hat{K}(\sigma - \sigma') \hat{f}(\tau;\sigma_1) \hat{f}\left( \tau; \frac{\sigma' - m\sigma_1}{1-m} \right) \frac{d\sigma_1}{1-m} d\sigma' d\tau, \\ \frac{\partial \hat{f}}{\partial \tau} &= \frac{\sigma \mathcal{H}(\tau - \sigma) \hat{n}(T;\sigma)}{1 + \int_{-\infty}^{\infty} \hat{n}(T;\sigma') d\sigma'} - \hat{f}(\tau;\sigma) \left( \hat{\mu} + \int_{-\infty}^{\infty} \hat{f}(\tau;\sigma') d\sigma' \right). \end{aligned} \tag{2.2.9}$$

The nondimensional system has 7 parameters, $\gamma$, $\hat{\omega}$, $\hat{\mu}$, $m$, $\hat{t_0}$, $\hat{t_1}$, and $\sigma_{\hat{K}}^2$, whereas the original system had 12 parameters. For the remainder of this thesis we will use only

the nondimensionalized model above. Hence, since no confusion can arise we rewrite the system using the original notation

$$N(T+1;s) = \gamma N(T;s) + \omega S(T;s), \tag{2.2.10a}$$

$$S(T;s) = \int_{t_0}^{t_1} \int_{-\infty}^{\infty} \int_{-\infty}^{\infty} K(s-s')F(t;s_1)F\left(t; \frac{s'-ms_1}{1-m}\right) \frac{ds_1}{1-m} ds' dt, \tag{2.2.10b}$$

$$\frac{\partial}{\partial t}F(t;s) = \frac{s\mathcal{H}(t-s)N(T;s)}{1+\int_{-\infty}^{\infty} N(T;s')ds'} - F(t;s)\left(\mu + \int_{-\infty}^{\infty} F(t;s')s'\right). \tag{2.2.10c}$$

In table 2.2 we present the default parameters we will use for numerical simulation throughout this thesis. We chose these particular parameters because they produced interesting results for both approaches (chapters 3 and 4). We conducted simulations for a variety of parameters and reported those where significantly different behaviour was observed.

Table 2.2: Default nondimensional parameter values

| **Parameter** | **Value** |
|---|---|
| $t_0$ | 0 |
| $t_1$ | 60 |
| $\mu$ | 0.5 |
| $m$ | 0 |
| $\gamma$ | 0.2 |
| $\omega$ | 0.9 |

## 2.3 Local stability of the extinction state

We formally linearize (2.2.10) at the zero steady state. Our calculations indicate that the state is likely locally asymptotically stable. We will prove this in the special case of the adaptive dynamcis approach in the next chapter.

A steady state of (2.2.10), denoted by $(N^*, F^*)$, is a solution of

$$\begin{aligned} N^*(s) &= \gamma N^*(s) + \omega S^*(T;s), \\ \frac{\partial}{\partial t}F^*(t;s) &= \frac{s\mathcal{H}(t-s)N^*(s)}{1+\int_{-\infty}^{\infty} N^*(s)} - \mu F^*(t;s) - F^*(t;s)\int_{-\infty}^{\infty} F^*(t;s')s', \quad F^*(t_0;s) = 0. \end{aligned} \tag{2.3.1}$$

For some small $\epsilon > 0$, a nearby solution can be written as

$$\begin{aligned} N(T;s) &= N^*(s) + \epsilon n(T;s) + \text{h.o.t}, \\ F(t;s) &= F^*(t;s) + \epsilon f(t;s) + \text{h.o.t}, \\ S(T;s) &= S^*(T;s) + \epsilon \tilde{S}(T;s) + \text{h.o.t}. \end{aligned} \tag{2.3.2}$$

Substituting (2.3.2) in (2.2.10), we get

$$\begin{aligned} N(T+1;s) &= N^*(s) + \epsilon n(T+1;s) + \text{h.o.t} \\ &= \gamma N^*(s) + \omega S^*(T;s) + \epsilon(\gamma n(T;s) + \omega \tilde{S}(T;s)) + \text{h.o.t} \\ \frac{\partial}{\partial t}F(t;s) &= \frac{\partial}{\partial t}F^*(t;s) + \epsilon \frac{\partial}{\partial t} f(t;s) + \text{h.o.t} \\ &= \frac{s\mathcal{H}(T-s)N^*(s)}{1+\int_{-\infty}^{\infty} N^*(s)ds} - \mu F^*(t;s) - F^*(t;s)\int_{-\infty}^{\infty} F^*(t;s')ds' \\ &\quad + \epsilon \left( \frac{s\mathcal{H}(t-s)\left(n + n\int_{-\infty}^{\infty} N^*(s)ds - N^*(s)\int_{-\infty}^{\infty} n(T;s)ds\right)}{\left(1+\int_{-\infty}^{\infty} N^*(s)ds\right)^2} - \mu f(t;s) \right) \\ &\quad - \epsilon \left( F^*(t;s)\int_{-\infty}^{\infty} f(t;s')ds' + f(t;s)\int_{-\infty}^{\infty} F^*(t;s')ds' \right) \\ &\quad - \epsilon^2 s\mathcal{H}(t-s) \left( \frac{n(T;s)\int_{-\infty}^{\infty} n(T;s)ds}{\left(1+\int_{-\infty}^{\infty} N^*(s)ds\right)^2} - \frac{N^*(s)\left(\int_{-\infty}^{\infty} n(T;s)ds\right)^2}{\left(1+\int_{-\infty}^{\infty} N^*(s)ds\right)^3} \right) \\ &\quad - \epsilon^2 f(t;s)\int_{-\infty}^{\infty} f(t;s')ds' + \text{h.o.t} \end{aligned} \tag{2.3.3}$$

We write $\hat{S}(t) = \hat{S}^*(t) + \epsilon\tilde{S}(t) + \text{h.o.t}$. We get

$$\begin{aligned} \frac{d}{dt}\hat{S}(t) &= \frac{d}{dt}\hat{S}^*(t) + \epsilon\frac{d}{dt}\tilde{S}(t) + \text{h.o.t} \\ &= \int_{-\infty}^{\infty}\int_{-\infty}^{\infty} F(t;s_1)F(t;s_2)ds_1ds_2 \\ &= \int\int F^*(s_1)F^*(s_2)ds_1ds_2 + \epsilon\int\int \left(F^*(s_1)f(t;s_2) + f(t;s_1)F^*(s_2)\right)ds_1ds_2 \\ &\quad + \epsilon^2\int\int f(t;s_1)f(t;s_2)ds_1ds_2 + \text{h.o.t}. \end{aligned} \tag{2.3.4}$$

We compare powers of $\epsilon$. For $\epsilon^0$, we get the steady state equations in (2.3.1). For $\epsilon^1$,

we obtain

$$\begin{aligned} n(T+1;s) &= \gamma n(T;s) + \omega \tilde{S}(T;s), \\ \frac{d}{dt}\tilde{S}(t) &= \int_{-\infty}^{\infty}\int_{-\infty}^{\infty} (F^*(s_1)f(t;s_2) + f(t;s_1)F^*(s_2))\, ds_1 ds_2. \end{aligned} \tag{2.3.5}$$

We do not include the $f$ because its value does not affect the equation for $\tilde{S}(t)$ when we are studying the trivial steady state, wherein $(N^*, F^*) = (0,0)$. At this state, we get the ODE $\frac{d}{dt}\tilde{S}(t) = 0$, which has initial condtion $\tilde{S}(t_0) = 0$. Hence, $\tilde{S}(t) = 0$. Then, since $\tilde{S}(t_1) = \int \tilde{S}(t_1;s)ds$ and $\tilde{S}(T;s) = \int K(s-s')\tilde{S}(t_1;s')ds'$, we also get that $\tilde{S}(T;s) = 0$. Therefore, from (2.3.5), we have $n(T+1;s) = \gamma n(T;s)$ for $0 < \gamma < 1$. Thus, $n(T;s) \to 0$, so that solutions nearby the trivial steady state go towards it. Therefore, the zero steady state seems to be locally asymptotically stable.

Biologically, the stability of the zero steady state represents the presence of an Allee effect in the population [8]. Allee effects occur whenever the fitness of an individual in a small population decreases as the population size or density also declines [2]. An Allee effect could be generated by multiple factors, such as a lack of genetic variation, demographic variation, or pollinator limitations [9].

## 2.4 Numerical simulation

In this section, we simulate (2.2.10) using the parameters in table 2.2 for the simplest case, wherein $m = 0$. When $m = 0$, seedlings solely inherit the trait of one parent plant. For the probability of mutation we chose the Gaussian distribution with mean zero and variance $\sigma_K^2$. Equation (2.1.12) becomes

$$S(T;s) = \int_{-\infty}^{\infty} \frac{1}{\sqrt{2\pi\sigma_K^2}} e^{-\frac{(s-s')^2}{2\sigma_K^2}} \hat{S}(t_1;s')ds'. \tag{2.4.1}$$

In the actual model the integral was infinite, but in order to run numerical simulations we integrate only over $s$ values that are contained within the season. Hence, we simulate the model

$$\begin{aligned} N(T+1;s) &= \gamma N(T;s) \\ &\quad + \frac{\omega}{\sqrt{2\pi\sigma_K^2}} \int_0^{t_g}\int_{t_0}^{t_1}\int_0^{t_g} e^{-\frac{(s-s')^2}{2\sigma_K^2}} F(t;s_1)F(t;s')ds_1 dt ds', \\ \frac{\partial F(t;s)}{\partial t} &= \frac{s\mathcal{H}(t-s)N(T;s)}{1+\int_0^{t_g} N(T;s')ds'} - F(t;s)\left(\mu + \int_0^{t_g} F(t;s')ds'\right). \end{aligned} \tag{2.4.2}$$

We discretize the interval $(0, t_g)$ with a regular grid and denote gridpoints by $s_j$, $j = 1, ..., J$. Given $N(T;s_j)$ for all $j$, we solve the $J$ differential equations for

$F(t; s_j)$ by discretizing time and using a simple forward Euler method. Since the dynamcis of the $F$-equations are simple and monotone, this method proved to be sufficiently accurate and fast. All integrals were approximated as Riemann sums. Given the solutions of $F(t; s_j)$, $j = 1, ...J$, we then calculated the updated values for $N(T + 1; s_j)$ for all $j$.

In figure 2.2, we plot the plant population, $N(T; s)$, as a function of flowering onset, $s$, and time, $T$, for $m = 0$. We observe that over time the population seems to reach some steady state. The peak of the distribution appears to occur at an intermediary flowering time.

In figure 2.3, we plot the plant population $N(T; s)$ as a function of $s$, after the final time step, $T = 100$, for varying $\sigma_K^2$. We observe that the distribution narrows as the mutation variance decreases. Hence, as mutation variance decreases, the distribution of flowering times seems to be converging to a Dirac delta distribution. In other words, the population is becoming monomorphic over time when mutation variance is low and reproduction is clonal. This suggests that the adaptive dynamics approach is a valid method of analysis for our model.

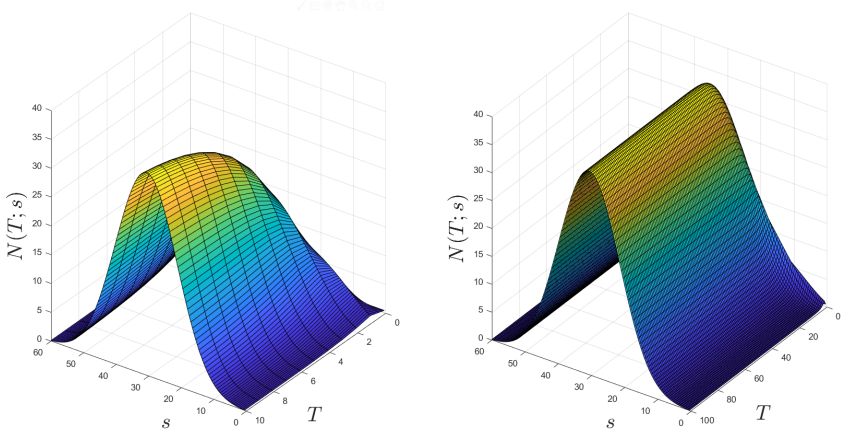


Figure 2.2: $N(T; s)$ as a function of flowering onset, $s$, and time, $T$, for $T = 10$ and $T = 100$. Parameters are as in table 2.2 with $m = 0$ and $\sigma^2 = 15$. The initial population is chosen such that $\bar{N}(0) = 50$.

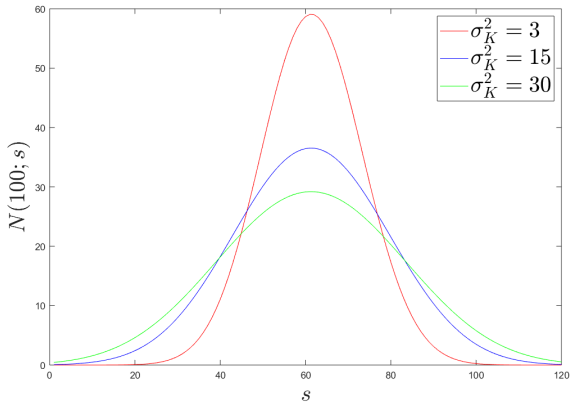


Figure 2.3: $N(T; s)$ as a function of flowering onset, $s$, at $T = 100$ for different values of $\sigma_K^2$. Parameters are as in table 2.2 with $m = 0$. The initial population is chosen such that $\bar{N}(0) = 50$.

# Chapter 3

# Adaptive dynamics approach

In this chapter, we apply the adaptive dynamics approach from section 1.3 to our model. Our model contains both ecological and evolutionary components. Adaptive dynamics separates these two aspects by assuming that the ecological dynamics are fast compared to the evolutionary dynamics. We identify the relevant processes and make the required assumptions to obtain an appropriate model for the ecological dynamics. We then apply the adaptive dynamics approach to evaluate the evolutionary component.

Since adaptive dynamics assumes that offspring are identical to their parents, we set $m = 0$ in (2.1.9). The theory also assumes that mutations are small and occur only on the slower evolutionary time scale. To represent this in our model, we use the Dirac delta distribution for the mutation kernel. Hence, we have

$$S(T;s) = \hat{S}(t_1;s) = \int_{t_0}^{t_1} F(t;s) \left( \int_{-\infty}^{\infty} F(t;s_1) ds_1 \right) dt. \tag{3.0.1}$$

To begin, we assume that our population is monomorphic with only one trait value. Then all mass of $N(T;s)$ is concentrated at a single point. This value, denoted by $s = s_x$ will be called the resident trait. We can write $N(T;s) = x_T \delta(s - s_x)$, where $\delta$ is the Dirac delta distribution and $x_T = \int_{-\infty}^{\infty} N(T;s) ds$ is the height of the distribution. Similarly, we write $F(t;s) = F(t)\delta(s - s_x)$, with $F(t) = \int_{-\infty}^{\infty} F(t;s) ds$ for unpollinated flowers with monomorphic trait. Upon introduction, the mutant population will have trait $s_y$, plant population $y_T \delta(s - s_y)$ and unpollinated flowers $H(t)\delta(s - s_y)$.

We consider the model with constant biomass growth rate as in (2.1.3). For the $F$ equation, we apply the above notation to (2.2.10c) and integrate over $s$. We get

$$\frac{d}{dt}F(t) = \frac{s_x \mathcal{H}(t - s_x) x_T}{1 + x_T} - F(t)(\mu + F(t)), \qquad t_0 < t < t_1, \;\; F(t_0) = 0. \tag{3.0.2}$$

From (3.0.1), we have

$$S(T) = \int_{t_0}^{t_1} F^2(t)\delta(s - s_x)dt. \tag{3.0.3}$$

Hence, applying the notation to (2.2.10a) and integrating over $s$, we get

$$x_{T+1} = \gamma x_T + \omega \int_{t_0}^{t_1} F^2(t)dt. \tag{3.0.4}$$

To simplify calculations we will start at $t_0 + s_x$ instead of $t_0$ so that the heaviside function is no longer necessary. Therefore, the resident population satisfies the hybrid system

$$\begin{aligned} \frac{d}{dt}F(t) &= \frac{s_x x_T}{1 + x_T} - F(t)(\mu + F(t)), \qquad t_0 + s_x < t < t_1, \;\; F(t_0 + s_x) = 0, \\ x_{T+1} &= \gamma x_T + \omega \int_{t_0+s_x}^{t_1} F^2(t)dt. \end{aligned} \tag{3.0.5}$$

In figure 3.1, we plot $x_{T+1}$ as a function of $x_T$ for two different parameter sets. In one case, we observe that the system has 3 steady states, and in the other case the system has only a single steady state at zero. Hence, simulations suggest that the resident system emits a fold bifurcation. This indicates that the populations ability to grow is heavily dependent upon its initial population density. In both cases, the updating function for $x_T$ appears to be monotonic. We prove this, as well as other properties of the resident system in the next section.

In figure 3.2, we plot the larger of the two positive steady states of (3.0.5), when it exists, as a function of $s_x$. We observe that the equilibrium, $x^*$, is highest when flowering begins roughly halfway through the season and lowest when flowering begins early or late. This illustrates the effect of the tradeoff described in section 1. In particular, for $\mu = 0.5$ and $t_g = 60$, $x^*$ was highest at $s_x = 30.62$.

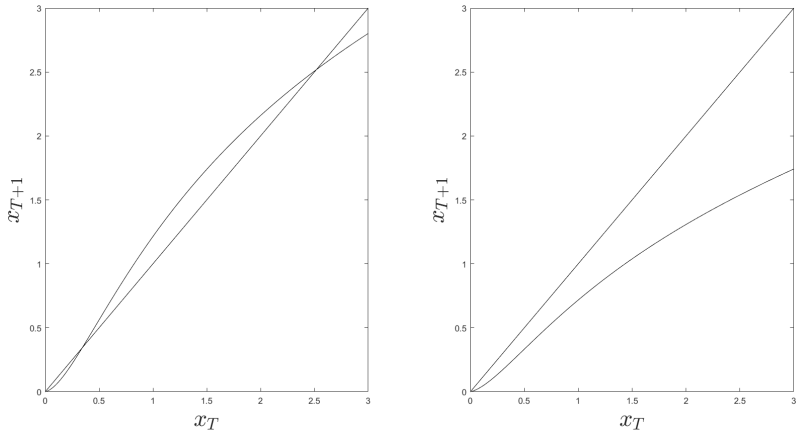


Figure 3.1: Plot of $x_{T+1}$ as a function of $x_T$ for two different parameter sets with $s_x = 1$. Parameters are as in table 2.2 with $\mu = 3.5$ (left) and $\mu = 5$ (right).

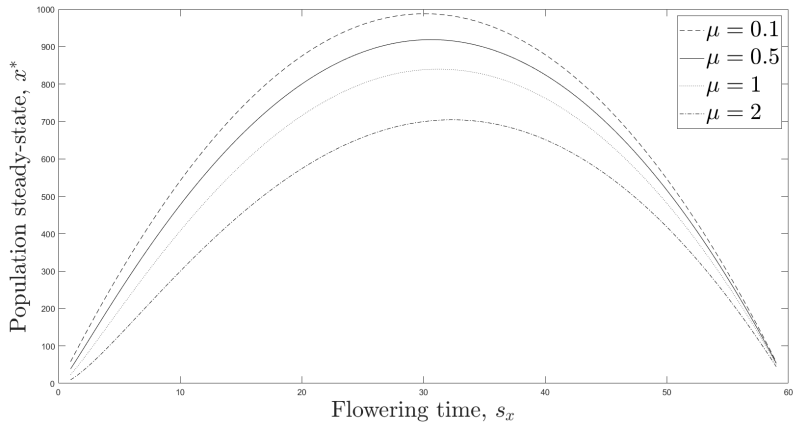


Figure 3.2: Plot of the larger of the two resident steady states, $x^*$, as a function of flowering time, $s_x$, for different values of $\mu$. Other parameters are as in table 2.2.

## 3.1 Properties of the resident system

**Lemma 3.1.1.** *The solution of (3.0.5), with initial condition $F(t_0+s_x)=0$, is given by*

$$F(t)=F_1\left[1-\frac{\mu+2F_1}{F_1+(\mu+F_1)e^{(\mu+2F_1)(t-(t_0+s_x))}}\right], \tag{3.1.1}$$

*where*

$$F_1=\frac{1}{2}\left(-\mu+\sqrt{\mu^2+\frac{4s_xx_T}{1+x_T}}\right). \tag{3.1.2}$$

**Proof:** The equation is a Ricatti equation with constant coefficients. We follow the standard steps to solve it. A constant solution of (3.0.5) satisfies

$$0=\frac{s_xx_T}{1+x_T}-\mu F_1-F_1^2. \tag{3.1.3}$$

The unique positive (i.e. biologically meaningful) solution is given by (3.1.2). As is standard for Ricatti equations, we now substitute $F=F_1+1/\bar{F}$ into (3.0.5). We get the ODE for $\bar{F}$

$$\frac{d\bar{F}}{dt}=(\mu+2F_1)\bar{F}+1. \tag{3.1.4}$$

The general solution for $\bar{F}$ is

$$\bar{F}=\frac{-1+c(\mu+2F_1)e^{(\mu+2F_1)t}}{\mu+2F_1}, \tag{3.1.5}$$

where $c$ is a constant. Inverting $\bar{F}$, we get the general solution for $F(t)$

$$F(t)=F_1+\frac{\mu+2F_1}{-1+c(\mu+2F_1)e^{(\mu+2F_1)t}}, \tag{3.1.6}$$

with $F_1$ as in (3.1.2). Applying the initial condition, we obtain the final solution (3.1.1). ∎

**Lemma 3.1.2.** *Solutions of (3.0.5) with non-negative initial conditions remain bounded, i.e. if $0<x_T<\infty$, then $0<x_{T+1}<M<\infty\ \forall T$, where $M$ depends only on system parameters.*

**Proof:** Firstly, we have that $\int_{t_0+s_x}^{t_1}F^2(t)dt>0$, $\omega>0$, and $\gamma>0$ so that if $x_T>0$, then

$$x_{T+1}=\gamma x_T+\omega\int_{t_0+s_x}^{t_1}F^2(t)dt>0. \tag{3.1.7}$$

Hence, solutions with non-negative initial conditions remain non-negative. By lemma 3.1.1, the solution of $F(t)$ is given by (3.1.1) where $F_1 > 0$ and $\mu > 0$. Hence, $F < F_1$, where $F_1$ is given by (3.1.2). We have the upper bound

$$\frac{x_T}{1+x_T} < 1, \tag{3.1.8}$$

so that

$$F < F_1 < \frac{1}{2}\left(-\mu + \sqrt{\mu^2 + 4s_x}\right) := C. \tag{3.1.9}$$

Hence, $F(t) < C$, for some $0 < C < \infty$ independent of $t$ or $T$. Then,

$$x_{T+1} < \gamma x_T + C^2(t_1 - t_0 - s_x) < \infty. \tag{3.1.10}$$

Thus, solutions of (3.0.5) with non-negative initial conditions remain bounded. Furthermore, we can define a sequence $\tilde{x}_T$ such that

$$\tilde{x}_{T+1} = \gamma \tilde{x}_T + C^2(t_1 - t_0 - s_x). \tag{3.1.11}$$

Then a steady state, $\tilde{x}^*$, of this system satisfies

$$\tilde{x}^* = \frac{C^2(t_1 - t_0 - s_x)}{1-\gamma}. \tag{3.1.12}$$

Furthermore, (3.1.10) is bounded by (3.1.11). Hence, a solution, $x_T$, of (3.0.5) is bounded by the maximum of $\tilde{x}^*$ and the initial condition, i.e.

$$x_T < \max\left(\frac{C^2(t_1 - t_0 - s_x)}{1-\gamma}, x_0\right). \tag{3.1.13}$$

∎

**Lemma 3.1.3.** *The recursion equation in (3.0.5) is monotone.*

**Proof:** Case 1: Assume $x_{T+1} > x_T$. We define $F$ in year $T$ and $T+1$ by $U$ and $V$, respectively. From (3.0.5), we have

$$\begin{aligned} \dot{U} &= \frac{d}{dt}U(t) = \frac{s_x x_T}{1+x_T} - \mu U(t) - U^2(t), \\ \dot{V} &= \frac{d}{dt}V(t) = \frac{s_x x_{T+1}}{1+x_{T+1}} - \mu V(t) - V^2(t), \end{aligned} \tag{3.1.14}$$

with $U(t_0 + s_x) = V(t_0 + s_x) = 0$. Furthermore, by assumption

$$\frac{s_x x_{T+1}}{1+x_{T+1}} > \frac{s_x x_T}{1+x_T}. \tag{3.1.15}$$

Then $\dot{V}(t_0+s_x) > \dot{U}(t_0+s_x)$. So $V(t) > U(t)$ in some interval $t_0+s_x < t < t_0+s_x+\epsilon$, where $\epsilon$ is sufficiently small. We want to prove that $V(t) > U(t)\ \forall t$.

Assume, towards a contradiction, that for some $t > t_0 + s_x + \epsilon$, $V(t) \leqslant U(t)$. Then there exists some $t^* > t_0 + s_x + \epsilon$ such that $V(t^*) = U(t^*)$, where $t^*$ is the smallest such $t > t_0 + s_x + \epsilon$. By (3.1.15), $\dot{U}(t^*) < \dot{V}(t^*)$ so that $V(t) < U(t)$ for some $t^* - \delta < t < t^*$, $\delta$ sufficiently small. However, we assumed that $U(t) \leqslant V(t)$ for $t < t^*$. Therefore, we have a contradiction. Thus, $V(t) > U(t)\ \forall t$, and

$$\begin{aligned} x_{T+2} &= \gamma x_{T+1} + \omega \int_{t_0+s_x}^{t_1} V^2(t)dt \\ &> \gamma x_T + \omega \int_{t_0+s_x}^{t_1} U^2(t)dt \\ &= x_{T+1}. \end{aligned} \tag{3.1.16}$$

Hence, $x_{T+1} > x_T \implies x_{T+2} > x_{T+1}$ so that the recursion equation is monotone increasing.
Case 2: Assume $x_{T+1} < x_T$. Following a similar argument as in case 1, we find $x_{T+2} < x_{T+1}$ so that the recursion equation is monotone decreasing.
In either case, the recursion equation in (3.0.5) is monotone. ∎

As a consequence of the previous two lemmas, we get lemma 3.1.4.

**Lemma 3.1.4.** *Solutions of (3.0.5) converge to either the zero steady state or some other positive steady state.*

**Lemma 3.1.5.** *The zero steady state of (3.0.5) is locally asymptotically stable.*

**Proof:** A steady state of (3.0.5), denoted by $(x^*, F^*)$, is a solution of

$$\begin{aligned} x^* &= \gamma x^* + \omega \int_{t_0+s_x}^{t_1} (F^*)(t)^2 dt, \\ \frac{dF^*(t)}{dt} &= \frac{s_x x^*}{1+x^*} - F^*(t)(\mu + F^*(t)). \end{aligned} \tag{3.1.17}$$

For some small $\epsilon > 0$, a nearby solution can be written as

$$\begin{aligned} x_T &= x^* + \epsilon \tilde{x}_T + \text{h.o.t}, \\ F(t) &= F^* + \epsilon f(t) + \text{h.o.t}. \end{aligned} \tag{3.1.18}$$

Substituting (3.1.18) into the recursion equation in (3.0.5), we get

$$\begin{aligned} x_{T+1} &= x^* + \epsilon\tilde{x}_{T+1} + \text{h.o.t} \\ &= \gamma x^* + \omega\int_{t_0+s_x}^{t_1}(F^*)^2(t)dt + \epsilon\left(\gamma\tilde{x}_T + 2\omega\int_{t_0+s_x}^{t_1}F^*(t)f(t)dt\right) \\ &+ \epsilon^2\omega\int_{t_0+s_x}^{t_1}f^2(t)dt + \text{h.o.t} \end{aligned} \tag{3.1.19}$$

We compare powers of $\epsilon$. For $\epsilon^0$, we get the steady state equation in (3.1.17). For $\epsilon^1$, we have

$$\tilde{x}_{T+1} = \gamma\tilde{x}_T + 2\omega\int_{t_0+s_x}^{t_1}F^*(t)f(t)dt. \tag{3.1.20}$$

Finding an equation for $f$ is not necessary since we are studying the trivial steady state, $(x^*, F^*) = (0, 0)$, so that $F^*(t)f(t) = 0$. Hence, we have that $\tilde{x}_{T+1} = \gamma\tilde{x}_T$ for some $0 < \gamma < 1$. Thus, $\tilde{x}_T \to 0$, so that that solutions nearby the trivial steady state go towards it. Therefore, the zero steady state of (3.0.5) is locally asymptotically stable. ∎

## 3.2 Invasion analysis

We now introduce the mutant population. The system for the resident and mutant populations together is

$$\begin{aligned} \frac{d}{dt}F(t) &= \frac{s_x x_T}{1+x_T+y_T} - \mu F(t) - F(t)(F(t)+H(t)), \\ x_{T+1} &= \gamma x_T + \omega\int_{t_0+s_x}^{t_1}F(t)(F(t)+H(t))dt, \\ \frac{d}{dt}H(t) &= \frac{s_y y_T}{1+y_T+x_T} - \mu H(t) - H(t)(H(t)+F(t)), \\ y_{T+1} &= \gamma y_T + \omega\int_{t_0+s_y}^{t_1}H(t)(H(t)+F(t))dt. \end{aligned} \tag{3.2.1}$$

Linearizing this system at the resident steady state, denoted by $(x^*, F^*(t))$, the mutant system becomes

$$\begin{aligned} \frac{d}{dt}H(t) &= \frac{s_y y_T}{1+x^*} - \mu H(t) - H(t)F^*(t), \\ y_{T+1} &= \gamma y_T + \omega\int_{t_0+s_y}^{t_1}H(t)F^*(t)dt. \end{aligned} \tag{3.2.2}$$

The mutant can grow if $y_1 > y_0$, and will die out if $y_1 < y_0$ [10]. We define the invasion exponent for the hybrid model as

$$I(s_x, s_y) = \frac{y_1}{y_0}, \tag{3.2.3}$$

A mutant with trait $s_y$ can invade the resident when $I(s_x, s_y) > 1$ and is unsuccessful if $I(s_x, s_y) < 1$.

As in section 1.3, we assume that mutations are small so that $s_y = s_x + \epsilon$, for $|\epsilon| << 1$. Expanding $I(s_x, s_y)$ in a Taylor series with respect to $\epsilon$, we get

$$I(s_x, s_y) = I(s_x, s_x) + \frac{\partial}{\partial s_y} I(s_x, s_x)\epsilon + \frac{\partial^2}{\partial {s_y}^2} I(s_x, s_x)\frac{\epsilon^2}{2!} + \dots. \tag{3.2.4}$$

At the resident steady state we have $I(s_x, s_x) = 1$. Thus, for $\epsilon$ small enough, $I(s_x, s_y) > 1$ as long as the selection gradient is positive, i.e.

$$\frac{\partial}{\partial s_y} I(s_x, s_y)\Big|_{s_y = s_x} > 0. \tag{3.2.5}$$

Hence, for our hybrid model the sign of the selection gradient once again indicates the direction in which a trait will evolve from the resident strategy. Singular points for the hybrid model can be classified according to the theory outlined in section 1.3.3.

The invasion exponent for our model is

$$I(s_x, s_y) = \gamma + \frac{\omega}{y_0} \int_{t_0 + s_y}^{t_1} F^*(t) H(t) dt. \tag{3.2.6}$$

The corresponding selection gradient can be calculated analytically in terms of $F^*(t)$ and $x^*$. The mutant equation (3.2.2) has the solution

$$H(t) = \frac{s_y y_0}{1 + x^*} \int_{t_0 + s_y}^{t} e^{-\int_\tau^t (\mu + F^*(z))dz} d\tau. \tag{3.2.7}$$

This gives us the selection gradient

$$\begin{aligned} \frac{\partial}{\partial s_y} I(s_x, s_y)\Big|_{s_y = s_x} &= \frac{\partial}{\partial s_y} \left( \frac{\omega}{y_0} \int_{t_0 + s_y}^{t_1} F^*(t) H(t) dt \right) \Big|_{s_y = s_x} \\ &= \frac{\omega}{1 + x^*} \frac{\partial}{\partial s_y} \left( s_y \int_{t_0 + s_y}^{t_1} F^*(t) \left( \int_{t_0 + s_y}^{t} e^{-\int_\tau^t (\mu + F^*(z))dz} d\tau \right) dt \right) \Big|_{s_y = s_x}. \end{aligned} \tag{3.2.8}$$

Using the product rule, we have

$$\frac{\partial}{\partial s_y} I(s_x, s_y)\Big|_{s_y=s_x} = \frac{\omega}{1+x^*}\int_{t_0+s_y}^{t_1} F^*(t)\left(\int_{t_0+s_y}^{t} e^{-\int_\tau^t(\mu+F^*(z))dz}d\tau\right)dt\Big|_{s_y=s_x} + \frac{\omega s_y}{1+x^*}\frac{\partial}{\partial s_y}\int_{t_0+s_y}^{t_1} F^*(t)\left(\int_{t_0+s_y}^{t} e^{-\int_\tau^t(\mu+F^*(z))dz}d\tau\right)dt\Big|_{s_y=s_x} \tag{3.2.9}$$

For the first term, letting $s_y = s_x$, we get

$$\frac{\omega}{1+x^*}\int_{t_0+s_x}^{t_1} F^*(t)\left(\int_{t_0+s_y}^{t} e^{-\int_\tau^t(\mu+F^*(z))dz}d\tau\right)dt. \tag{3.2.10}$$

Adaptive dynamics assumes that the resident and mutant populations differ only in our trait value. Thus, at $s_y = s_x$, and $y_T = x^*$, we have that $H(t) = F^*(t)$. Hence,

$$\frac{1}{1+x^*}\left(\int_{t_0+s_y}^{t} e^{-\int_\tau^t(\mu+F^*(z))dz}d\tau\right) = \frac{F^*(t)}{s_x x^*}, \tag{3.2.11}$$

such that the first term in (3.2.9) for the selection gradient is

$$\frac{\omega}{s_x x^*}\int_{t_0+s_x}^{t_1}(F^*)^2(t)dt. \tag{3.2.12}$$

For the second term in (3.2.9), we use *Leibniz rule of integration.* Since $F^*(t)$ is independent of $s_y$, we have

$$\frac{\omega s_y}{1+x^*}\int_{t_0+s_y}^{t_1} F^*(t)\frac{\partial}{\partial s_y}\left(\int_{t_0+s_y}^{t} e^{-\int_\tau^t(\mu+F^*(z))dz}d\tau\right)dt. \tag{3.2.13}$$

Applying Leibniz rule a second time, we get

$$\begin{aligned}\frac{\partial}{\partial s_y}\int_{t_0+s_y}^{t} e^{-\int_\tau^t(\mu+F^*(z))dz}d\tau &= \int_{t_0+s_y}^{t}\frac{\partial}{\partial s_y}e^{-\int_\tau^t(\mu+F^*(z))dz}d\tau - e^{-\int_{t_0+s_y}^t(\mu+F^*(z))dz} \\ &= -e^{-\int_{t_0+s_y}^t(\mu+F^*(z))dz}.\end{aligned} \tag{3.2.14}$$

Thus, at $s_y = s_x$, the second term in (3.2.9) is

$$-\frac{\omega s_x}{1+x^*}\int_{t_0+s_x}^{t_1} F^*(t)e^{-\int_{t_0+s_x}^t(\mu+F^*(z))dz}dt. \tag{3.2.15}$$

Therefore, the selection gradient is

$$\frac{\partial}{\partial s_y} I(s_x, s_y)\Big|_{s_y=s_x} = \frac{1-\gamma}{s_x} - \frac{\omega s_x}{1+x^*}\int_{t_0+s_x}^{t_1} F^*(t)e^{-\int_{t_0+s_x}^t(\mu+F^*(z))dz}dt. \tag{3.2.16}$$

**Lemma 3.2.1.** *A singular point of (3.2.16) is an ESS.*

**Proof:** As shown in section 1.3.3, a singular point, $\bar{s}$, is an ESS if $c_{22} < 0$ for $s_y = s_x = \bar{s}$. Taking the derivative of (3.2.9) again, we get

$$c_{22} = \frac{\partial^2}{\partial s_y^2} I(s_x, s_y)\Big|_{s_y=s_x=\bar{s}} = -\frac{(2+\mu\bar{s})\omega}{1+x^*} \int_{t_0+\bar{s}}^{t_1} F^*(t) e^{-\int_{t_0+\bar{s}}^{t} (\mu + F^*(z))dz} dt. \quad (3.2.17)$$

Hence, given that all parameters in our model are positive, $c_{22} < 0$. Therefore $\bar{s}$ is an ESS. ∎

Although we can formally calculate the coefficients $c_{11}$ and $c_{12}$, we cannot simplify them sufficiently to check the remaining possibilities for the singular strategy from section 1.3.3 analytically. Instead, we generate the PIP numerically and use the geometric criteria from section 1.3.3 to further classify the singular strategy.

We calculate the singular point of (3.2.16) numerically, using the default parameters in table 2.2, and find $\bar{s} = 30.96$. This value is slightly higher than midway through the season, which has length $t_g = 60$. We find that the singular point is both an ESS and a CSS. However, the singular strategy cannot invade other strategies, which means that it cannot be reached in a single mutation step. Additionally, mutual invasibility does not occur. In figure 3.3, we present the PIP for our system with parameter values in table 2.2. In figure 3.4, we evaluate the singular point based on the geometric criteria in section 1.3.3.

Other PIPs were constructed by varying parameters individually. We observed that the PIP only differed significantly when $\mu$ was altered, and showed little change for other parameters. We present PIPs for two alternate values of $\mu$ in figure 3.5. Although the PIPs look different overall, local behaviour was the same as that presented in figure 3.4 when focusing in on the singular point. This was consistent for all tested parameter values.

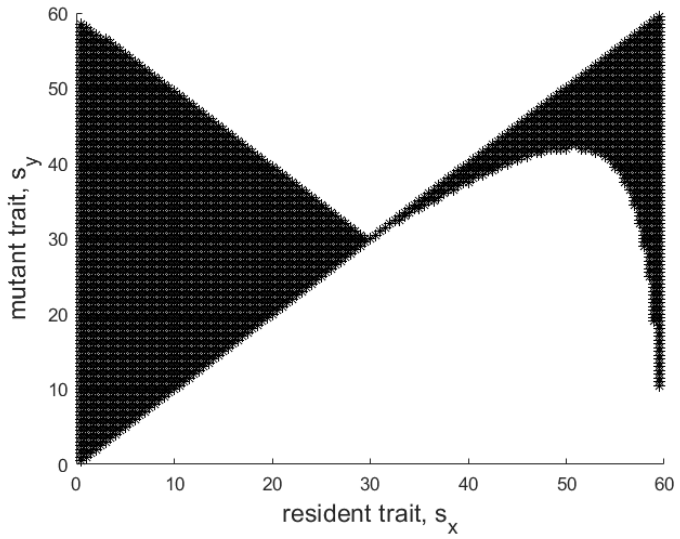


Figure 3.3: PIP for model (3.2.1) with parameters as in table 2.2. The singular point is numerically calculated to be $\bar{s} = 30.96$.

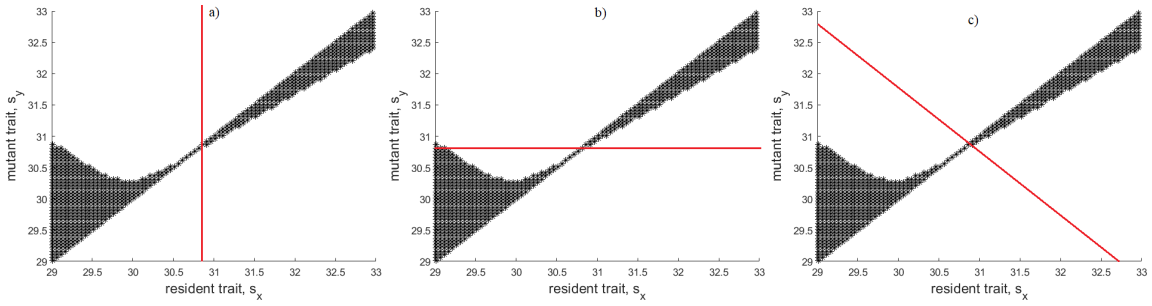


Figure 3.4: Closeup of the PIP in figure 3.3 around $\bar{s} = 30.96$. Geometrically we confirm that a) $\bar{s}$ is an ESS, b) $\bar{s}$ cannot invade nearby strategies, and c) mutual invasibility does not occur.

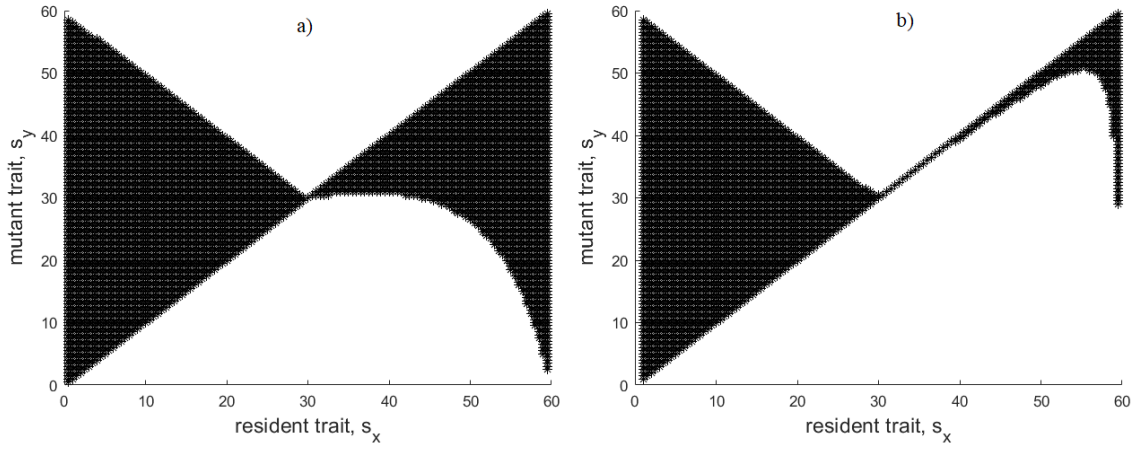


Figure 3.5: PIP for model (3.2.1) for a) $\mu = 0.1$, and b) $\mu = 2$. Other parameters are as in table 2.2.

# Chapter 4

# Moments approach

In the previous chapter, we applied the Adaptive Dynamics approach to our model. Under this method, the population was monomorphic, meaning that all individuals had the same flowering time. This simplification allowed us to obtain some explicit results for our complex model. In this chapter, we consider a different simplification, based on moment approximations. Deriving equations for moments is a fairly standard approach to dealing with complicated systems that describe physical or biological densities. However, we will see that our model leads to non-standard moment equations and requires slightly different ideas for moment closure.

We apply this approach to our original model derived in section 2.1, by assuming that our plant population represents a continuous distribution of flowering times. Under some additional assumptions, we obtain an approximate set of equations for the total population density (zero moment), and the mean flowering time (first moment). We then solve these equations numerically.

## 4.1 Derivation of the moment equations

As in the general model, we begin with $N(T; s)$, the plant population with flowering time $s$ in year $T$. As described in section 2.1, we can set the plant and flower populations to zero for $s \notin [0, t_g]$. Hence, all integrals involving $s$ will be taken over the entire real line.

The $i$-th raw moment of the density $N$, with respect to flowering time, is given by

$$M_N^i(T) = \int_{-\infty}^{\infty} s^i N(T; s) ds. \tag{4.1.1}$$

In particular, $M_N^0(T)$ is the total density of plants, which we will also denote as

$$\bar{N}(T) = \int_{-\infty}^{\infty} N(T; s) ds. \tag{4.1.2}$$

We denote moments of the other densities in the same manner, as $M_F^i(t)$ and $M_S^i(T)$. The total density of flowers and seeds will be denoted by $\bar{F}(t)$ and $\bar{S}(T)$ accordingly. The mean flowering time of plants in year $T$ is then given by

$$\mu_N(T) = \frac{M_N^1(T)}{\bar{N}(T)}. \tag{4.1.3}$$

We integrate equation (2.1.1) to obtain the recursion equation for the total plant density as

$$\bar{N}(T+1) = \gamma \bar{N}(T) + \omega \bar{S}(T). \tag{4.1.4}$$

Similarly, we take the first moments in (2.1.1) and find

$$M_N^1(T+1) = \gamma M_N^1(T) + \omega M_S^1(T). \tag{4.1.5}$$

In order to get $\bar{S}(T)$ and $M_S^1(T)$, we apply moments to the within-year equations. Using (2.2.10), we find

$$\begin{aligned} \frac{d}{dt}\bar{F}(t) &= \int_{-\infty}^{\infty} \frac{\partial}{\partial t} F(t;s) ds \\ &= \int_{-\infty}^{\infty} \left( B(t_0+s;s)\mathcal{H}(t-s)\frac{N(T;s)}{1+\bar{N}(T)} - \mu F(t;s) - \bar{F}(t)F(t;s) \right) ds \\ &= \frac{\int_{-\infty}^{t} B(t_0+s;s)N(T;s)ds}{1+\bar{N}(T)} - \mu \bar{F}(t) - \bar{F}^2(t), \end{aligned} \tag{4.1.6}$$

with initial condition $\bar{F}(t_0) = 0$. With constant growth rate as in (2.1.3), we get the nonautonomous Ricatti equation

$$\frac{d}{dt}\bar{F}(t) = \frac{\int_{-\infty}^{t} sN(T;s)ds}{1+\bar{N}(T)} - \mu \bar{F}(t) - \bar{F}^2(t). \tag{4.1.7}$$

Similarly, we find an ODE for the first raw moment, $M_F^1(t)$,

$$\begin{aligned} \frac{d}{dt}M_F^1(t) &= \int_{-\infty}^{\infty} s\frac{\partial}{\partial t} F(t;s) ds \\ &= \frac{\int_{-\infty}^{t} sB(t_0+s;s)N(T;s)ds}{1+\bar{N}(T)} - M_F(t)(\mu + \bar{F}(t)), \end{aligned} \tag{4.1.8}$$

with initial condition $M_F^1(t_0) = 0$. With constant growth rate, we get

$$\frac{d}{dt}M_F^1(t) = \frac{\int_{-\infty}^{t} s^2 N(T;s)ds}{1+\alpha\bar{N}(T)} - M_F(t)(\mu + \bar{F}(t)). \tag{4.1.9}$$

The density of seeds with trait $s$ is given by the convolution

$$S(T;s) = \int_{-\infty}^{\infty} K(s-s')\hat{S}(t_1;s')ds', \tag{4.1.10}$$

where $\hat{S}(t_1;s')$ is described in (2.1.11). For the total density, we get

$$\begin{aligned}
\bar{S}(T) &= \int_{-\infty}^{\infty} S(T;s)ds \\
&= \int_{-\infty}^{\infty} \left( \int_{-\infty}^{\infty} K(s-s')\hat{S}(t_1;s')ds' \right) ds \\
&= \int_{-\infty}^{\infty} K(y)dy \int_{-\infty}^{\infty} \hat{S}(t_1;s')ds' \\
&= \int_{-\infty}^{\infty} \left( \int_{t_0}^{t_1} \int_{-\infty}^{\infty} F(t;s_1) F\left(t; \frac{s'-ms_1}{1-m}\right) \frac{ds_1}{1-m} dt \right) ds' \\
&= \int_{t_0}^{t_1} \left( \int_{-\infty}^{\infty} F(t;s_1)ds_1 \int_{-\infty}^{\infty} F(t;y)dy \right) dt \\
&= \int_{t_0}^{t_1} \bar{F}^2(t)dt.
\end{aligned} \tag{4.1.11}$$

For the first moment, a similar calculation gives

$$M_S^1(T) = \int_{t_0}^{t_1} M_F^1(t)\bar{F}(t)dt, \tag{4.1.12}$$

where we have used the fact that $K$ has zero mean.

All together, we have derived the system of equations for the moments

$$\begin{aligned}
\bar{N}(T+1) &= \gamma \bar{N}(T) + \omega \int_{t_0}^{t_1} \bar{F}^2(t)dt, \\
M_N^1(T+1) &= \gamma M_N^1(T) + \omega \int_{t_0}^{t_1} M_F^1(t)\bar{F}(t)dt, \\
\frac{d}{dt}\bar{F}(t) &= \frac{\int_{-\infty}^{t} sN(T;s)ds}{1+\bar{N}(T)} - \mu\bar{F}(t) - \bar{F}^2(t), \\
\frac{d}{dt}M_F^1(t) &= \frac{\int_{-\infty}^{t} s^2 N(T;s)ds}{1+\bar{N}(T)} - M_F(t)(\mu + \bar{F}(t)).
\end{aligned} \tag{4.1.13}$$

As is common with this approach, our moments system is not closed. We discuss one way to close the system in the next section.

## 4.2 Moment closure

In general, the approach to deal with such a set of moment equations is to assume some sort of moment closure (for example by assuming that a certain moment is zero or constant) [24]. Such an approach cannot be directly applied to our system because the integral terms in (4.1.13) range from $-\infty$ to $t$ rather than over the full domain of the distribution. Instead, we proceed by assuming that the flowering times follow a particular probability distribution. Once a parametric form is fixed, we can calculate the integrals in (4.1.13), and analyze the behaviour of our system.

More specifically, we assume that

$$N(T;s) = \bar{N}(T)G(s), \tag{4.2.1}$$

where $G(s)$ is the probability density function of the chosen distribution. The $i$-th raw moment of $N(T;s)$ is then

$$M_N^i(T) = \int_{-\infty}^{\infty} s^i N(T;s)ds = \bar{N}(T)\int_{-\infty}^{\infty} s^i G(s)ds, \tag{4.2.2}$$

and the total density remains $\bar{N}(T) = M_N^0(T)$.

Under assumption (4.2.1), (4.1.13) becomes

$$\begin{aligned}
\bar{N}(T+1) &= \gamma\bar{N}(T) + \omega\int_{t_0}^{t_1}\bar{F}^2(t)dt,\\
M_N^1(T+1) &= \gamma M_N^1(T) + \omega\int_{t_0}^{t_1} M_F^1(t)\bar{F}(t)dt,\\
\frac{d}{dt}\bar{F}(t) &= \frac{\bar{N}(T)}{1+\bar{N}(T)}\int_{-\infty}^{t} sG(s)ds - \mu\bar{F}(t) - \bar{F}^2(t),\\
\frac{d}{dt}M_F^1(t) &= \frac{\bar{N}(T)}{1+\bar{N}(T)}\int_{-\infty}^{t} s^2G(s)ds - M_F^1(t)(\mu+\bar{F}(t)),
\end{aligned} \tag{4.2.3}$$

where $G(s)$ has parameters dependent upon the moments of the chosen distribution. For example, suppose we chose the exponential distribution for $G(s)$. Then, we have $G(s;\lambda(T)) = \lambda(T)e^{-\lambda(T)s}$, where $1/\lambda(T)$ is the mean. The distribution would then update from year to year according to the equation

$$\lambda(T+1) = \frac{1}{\mu_N(T+1)} = \frac{\bar{N}(T+1)}{M_N^1(T+1)}, \tag{4.2.4}$$

where $M_N^1(T+1)$ and $\bar{N}(T)$ are determined by (4.2.3).

## 4.3 Simulation results

In order to numerically simulate the moments model (4.2.3), we choose a distribution, $G(s)$. Although many distributions are possible, we choose the Gamma distribution because experimental studies have found that the onset of flowering appears most often to be Gamma distributed [15, 16]. We write the probability density function of the Gamma distribution in the modified form [23]

$$G(s;k,n) = \frac{kn}{\Gamma(n)}(kns)^{n-1}e^{-nks}, \tag{4.3.1}$$

where $n = n(T)$ is the shape parameter and $1/k$ ($k = k(T)$) is the mean. We update the parameters of our distribution according to the equations

$$k(T+1) = \frac{1}{\mu_N(T+1)} = \frac{\bar{N}(T+1)}{M_N^1(T+1)}, \qquad n(T+1) = \frac{(M_N^1(T+1))^2}{\bar{N}^2(T+1)\sigma_N^2(T+1)}, \tag{4.3.2}$$

where $k$ and $n$ are found by applying using the standard formulas for the mean ($\mu_N = 1/k$) and variance ($\sigma_N^2 = 1/nk^2$) of a Gamma distribution.

We assume that the variance, $\sigma_N^2$, is constant, choose an initial $\bar{N}(0)$ and $M_N^1(0)$ and update $k(T)$ and $n(T)$ in the Gamma distribution according to the derived recursion equations. In order to perform simulations, all infinite integrals in (4.1.13) are calculated only for $s$ values that are contained within the season, i.e. from $t_0$ to $t_g$. By choosing sufficiently small variance, the distribution is concentrated close to the mean so we can assume that loss on the boundary will be minimal. This is consistent with the biology that motivates our system. Flowering is impossible before emergence, and any plant that would flower after the season ends will not produce seeds for dispersal.

In figures 4.1 and 4.2, we plot the distribution of flowering times, $N(T;s)$, as a function of $s$ with different initial conditions. We observe that over time, the mean of the distribution appears to be approaching the halfway point of the season, although it may take many years to reach its equilibrium.

In figure 4.3 we plot the change in plant density $\bar{N}(T)$ and mean flowering time $\mu_N(T)$ for different season lengths. In all simulations, we observe convergence to a steady state. At this steady state, the mean flowering time appears to be around half the season length. Plant density is positive only when the season length is greater than the initial mean flowering time. For the default parameters in table 2.2. the equilibrium mean flowering time was $\mu_N^* = 30.2978$ which is around the middle of the season. This compares well with the adaptive dynamics method where we simulated the ESS to be $\bar{s} = 30.96$.

In figure 4.4 we plot the equilibrium mean flowering time and density, $\mu_N^*$ and $\bar{N}^*$, as functions of the season length for different values of $\mu$. The death rate $\mu$ was found to have a negative relationship with plant density, as expected, but to have

a positive relationship with mean flowering time. This occurs because with a lower plant population, flowers must remain open longer before they can find a pollen match and thus will flower later.

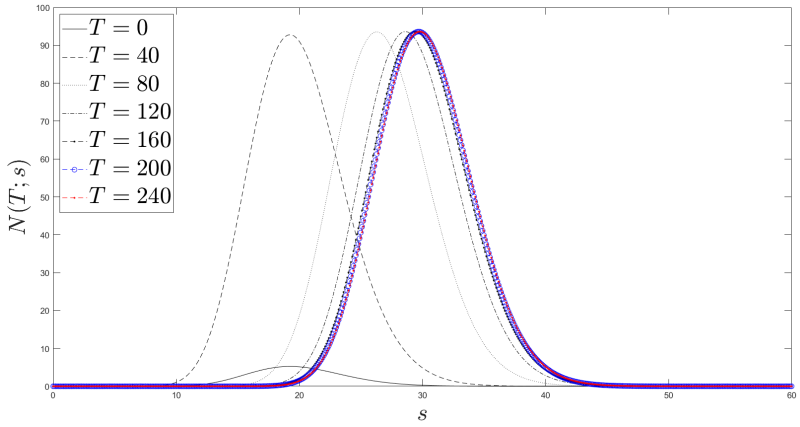


Figure 4.1: Plot of $N(T;s)$ as a function of $s$ for $t_g = 60$. Parameters are as in table 2.2, with variance $\sigma_N^2 = 15$. We chose initial conditions $\mu_N(0) = 20$, and $\bar{N}(0) = 50$.

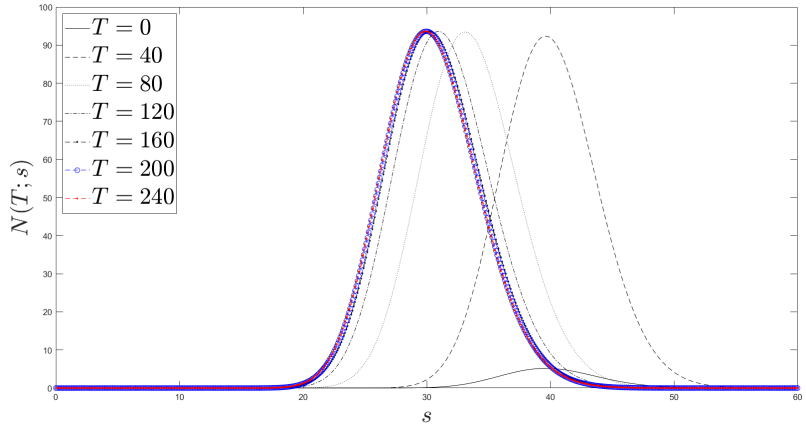


Figure 4.2: Plot of $N(T;s)$ as a function of $s$ for $t_g = 60$. Parameters are as in table 2.2, with variance $\sigma_N^2 = 15$. We chose initial conditions $\mu_N(0) = 40$, and $\bar{N}(0) = 50$.

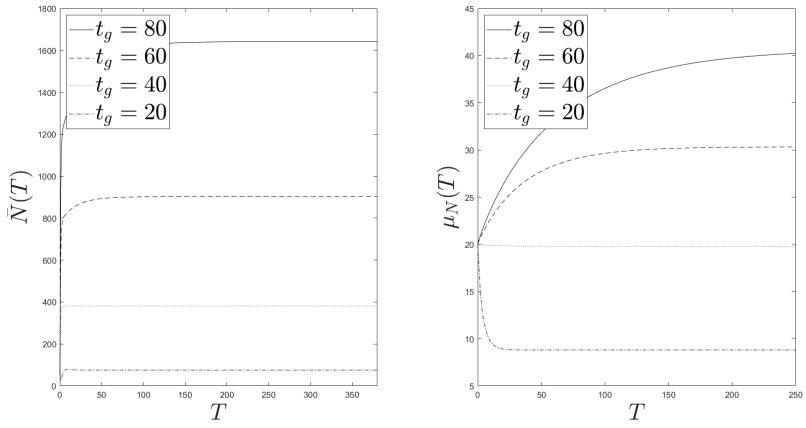


Figure 4.3: Plot of the change in plant density $\bar{N}(T)$ and mean flowering time $\mu_N(T)$ for different season lengths ($t_g = t_1 - t_0$). Parameters and initial values are as in figure 4.1.

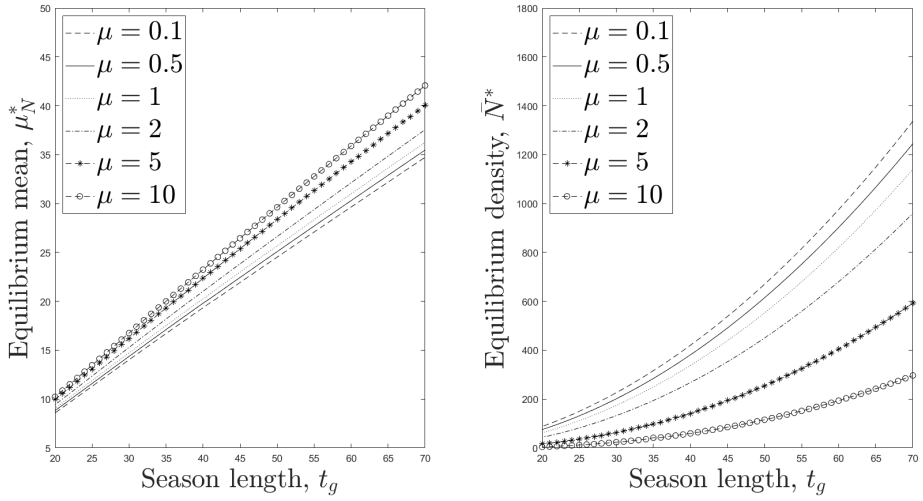


Figure 4.4: Plot of the equilibrium mean flowering time and density, $\mu_N^*$ and $\bar{N}^*$ as functions of the season length. Parameters and initial values are as in figure 4.1.

# Chapter 5

# Discussion

In this thesis, we studied the evolution of flowering time in perennial plants. Due to the trade-off between plant size and seed production we believed that there may be an optimal time for a plant to begin flowering. We hypothesized that this time would occur midway through the season. We created a mathematical model for the onset of flowering time in order to test this hypothesis. We also used our model to study the evolution of flowering time as a phenotype. We hoped to determine whether the trait value would evolve towards the middle of the season.

We created a novel hybrid integrodifferential model for the onset of flowering time in a perennial plant. We proved that the extinction state was locally stable, which indicated the presence of an Allee effect in our model (lemma **??**). The model was simulated for $m = 0$ using the Gaussian distribution to account for the probability of phenotype mutation within seeds. Due to the complexity of the model, further analytical and numerical results were unobtainable. Instead, we applied two simplifications that could be analyzed.

Two alternative methods were used to analyze the model: (1) the adaptive dynamics approach; and (2) the moments model. We applied the adaptive dynamics approach by rewriting our model for a monomorphic population. This simplified model had an analytical solution (lemma 3.1.1), that was monotone, and bounded (lemmas 3.1.3 and 3.1.2). This ensures that if the initial population is large enough it will converge to a positive steady state (lemma 3.1.4). This was confirmed numerically by plotting the update function of the resident system (figure 3.1). Simulating the resident model, towards the stable positive steady state, showed that the equilibrium population would be largest when flowering began roughly halfway through the season (figure 3.2). When performing invasion analysis, we were able to prove that the singular point is an ESS (lemma 3.2.1). Based on simulations, we also believe that this singular point will be convergent stable (figures 3.3 and 3.4) for all parameter values. In this case, the singular point is considered a continuously stable strategy and the population will evolve towards it.

For the second simplification to our model, we considered a population with a continuous distribution of flowering times. We derived equations for the moments of this distribution and rewrote our model in terms of the total population density and mean flowering time. Under the assumption that flowering time was Gamma-distributed, we looked at the change in mean flowering time and plant density for different season lengths (figures 4.3 and 4.4). In all cases, the mean flowering time evolved to approach the middle of the season. The season length, $t_g$, was found to have a positive relationship to both mean flowering time and population density. Using the same parameter values, the equilibrium mean flowering time of the moments approach was very similar to the ESS value of the adaptive dynamics approach.

Comparing the two approaches, we were able to confirm our hypothesis that the population would evolve to have an intermediate flowering time. Under the adaptive dynamics approach, we also found that the singular strategy occured at an intermediate flowering time, and proved that this strategy was an ESS. Hence, once the singular point is established in the population, no further evolutionary change is possible through small mutations [18]. We also believe that the singular strategy will the convergent stable, meaning the trait will evolve towards this strategy. Hence, the adaptive dynamics approach suggests that an intermediate flowering time can be reached through evolution.

Moving forward there are several ways in which our model could be extended. In this thesis we were only able to present numerical results for the full model with $m = 0$. This was enough to justify the adaptive dynamics application, but it only represents the case in which reproduction is clonal. To further explore the dynamics of our model different heritability conditions should be considered. Hence, the an important next step would be to create numerical methods to simulate the program for any possible heritability proportion, $0 < m < 1$.

We also only analyzed the model for a constant biomass growth rate, as in (2.1.3). However, plant growth is often dependent upon many external factors, such as temperature. It is likely that biomass growth would be slower at the beginning of the season, when temperatures are lower, and faster later in the season, as temperatures increase. Additionally, our model assumes that plants immediately stop growing once flowering begins. In reality the plant will grow more slowly, as growth resources are allocated to flowering, but is unlikely to stop growing completely. To capture these dynamics in our model, we would use a biomass growth rate that is dependent upon temperature, and decreases over time when flowering begins.

We would also like to examine the evolution of the trait across space by including dispersal in our model. Due to differences in elevation and/or latitude, population phenology may differ depending upon location [3]. To study trait evolution across these environmental gradients, dispersal must be taken into account. Seeds are transported across environmental gradients by flowing wind and water or in soil which is moved by animals or machinery [6]. Pollination is also dependent upon space, with

pollen being transferred between flowers via wind and insect or other animal vectors. To include all aspects of dispersal in our model, we would introduce some location $z$, and track $N(T, z; s)$, $F(t, z; s)$ and $S(T, z; s)$ across both space and time. Dispersal kernels would be included for the seed portion of the $N$ equation and for pollination in the $F$ equation.

# Bibliography


[1] K.S. Bawa, T. Ingty, L.J. Revell, and K.N. Shivaprakash. Correlated evolution of flower size and seed number in flowering plants (monocotyledons). *Annals of Botany*, 123:181–190, 2019.

[2] L. Berec, E. Angulo, and F. Courchamp. Multiple Allee effects and population management. *Trends in Ecology and Evolution*, 22:185–191, 2007.

[3] S. Bewick, R.S. Cantrell, C. Cosner, and W. F. Fagan. How resource phenology affects consumer population dynamics. *The American Naturalist*, 187:151–166, 2016.

[4] K. Bolmgren and P. Cowan. Time-size tradeoffs: a phylogenetic comparative study of flowering time, plant height and seed mass in a north-temperate flora. *Oikos*, 117:424–429, 2008.

[5] Å. Brännström, J. Johansson, and N. Festenberg. The hitchhikers guide to adaptive dynamics. *Games*, 4:304–328, 2013.

[6] J.M. Bullock, K. Shea, and O. Skarpaas. Measuring plant dispersal: an introduction to field methods and experimental design. *Plant Ecology*, 186:217–234, 2006.

[7] N. Champagnat, R. Ferrière, and G. Ben Arous. The canonical equation of adaptive dynamics: A mathematical view. *Selection*, 2:73–83, 2002.

[8] F. Courchamp, L. Berec, and J. Gascoigne. *Allee Effects in Ecology and Evolution*, pages 1–15. Oxford University Press, Oxford, NY, 2008.

[9] F. Courchamp, T. Clutton-Brock, and B. Grenfell. Inverse density dependence and the Allee effect. *Trends in Ecology and Evolution*, 14:405–410, 1999.

[10] O. Diekmann. A beginners guide to adaptive dynamics. *Mathematical Modelling of Population Dynamics*, 63, 2003.

[11] G. Du and W. Qi. Trade-offs between flowering time, plant height, and seed size within and across 11 communities of a qinghaitibetan flora. *Plant Ecology*, 209:321–333, 2010.

[12] M. Durinx, J.A.J. Metz, and G. Meszéna. Adaptive dynamics for physiologically structured population models. *Journal of Mathematical Biology*, 56:673–742, 2008.

[13] I. Eshel. Evolutionary and continuous stability. *Journal of Theoretical Biology*, 103:99–111, 1983.

[14] I. Eshel and U. Motro. Kin selection and strong evolutionary stability of mutual help. *Theoretical Population Biology*, 19:420–433, 1981.

[15] G. Fox. Components of flowering time variation in a desert annual. *Evolution*, 44:1404–1423, 1990.

[16] G. Fox. Assortative mating and plant phenology: Evolutionary and practical consequences. *Evolutionary Ecology Research*, 5:1–18, 2003.

[17] S.A.H. Geritz and É. Kisdi. On the mechanistic underpinning of discrete-time population models with complex dynamics. *Journal of Theoretical Biology*, 228:261–269, 2004.

[18] S.A.H. Geritz, É. Kisdi, G. Meszéna, and J.A.J. Metz. Evolutionarily singular strategies and the adaptive growth and branching of the evolutionary tree. *Evolutionary Ecology*, 12:35–57, 1998.

[19] R.J. Hall, A. Hastings, and D.R. Ayres. Explaining the explosion: modelling hybrid invasions. *Proceedins of the Royal Society B: Biological sciences*, 273:1385–1389, 2006.

[20] A. Jensen. Dynamics of populations with nonoverlapping generations, continuous mortality, and discrete reproductive periods. *Ecological Modelling*, 74:305–309, 1994.

[21] J.M. Jiménez-Gómez, C. Alonso-Blanco, A. Borja, G. Anastasio, T. Angosto, R. Lozano, and J.M. Martinez-Zapater. Quantitative genetic analysis of flowering time in tomato. *Gemone*, 50:303–315, 2007.

[22] E. Jongejans, K. Shea, O. Skarpaas, D. Kelly, and S.P. Ellner. Importance of individual and environmental variation for invasive species spread: a spatial integral projection model. *Ecology*, 92:86–97, 2011.

[23] M. Kot. *Elements of Mathematical Ecology*, chapter Delay Models, pages 70–93. Cambridge University Press, New York, NY, 2001.

[24] C. Kuehn. *Control of Self-Organizing Nonlinear Systems*, chapter Moment Closure - A Brief Review, pages 253–271. Springer International Publishing, 2016.

[25] A. Lamsal and S.M. Welch. Modelling flowering time of rhododendron. *Journal of Hill Agriculture*, 7:231–236, 2016.

[26] S. Lion. Theoretical approaches in evolutionary ecology: Environmental feedback as a unifying perspective. *The American Naturalist*, 191:21–44, 2018.

[27] A. Mauer, V. Draba, Y. Jiang, F. Schnaithmann, R. Sharma, E. Schumann, B. Kilian, J.C. Reif, and K. Pillen. Modelling the genetic architecture of flowering time control in barley through nested association mapping. *BMC Genomics*, 16, 2015.

[28] C. Merow, J.P. Dahlgren, C.J.E. Metcalf, D.Z. Childs, M.E.K. Evans, E. Jongejans, S. Record, M. Rees, R. Salguero-Gómez, and S.M. McMahon. Advancing population ecology with integral projection models: a practical guide. *Methods in Ecology and Evolution*, 5:99–110, 2014.

[29] J.A.J. Metz, R.M. Nisbet, and S.A.H. Geritz. How should we define fitness for general ecological scenarios? *Trends in Ecology and Evolution*, 7:198–202, 1992.

[30] S.P. Otto and T. Day. *A Biologists Guide to Mathematical Modeling in Ecology and Evolution*, chapter Equilibria and Stability Analyses - Nonlinear Models with Multiple Variables, pages 294–337. Princeton, University Press, Princeton, NJ, 2007.

[31] E. Pachepsky, R.M. Nisbet, and W.W. Murdoch. Between discrete and continuous: consumer-resource dynamics with synchronized reproduction. *Ecology*, 89:280–288, 2008.

[32] L. Perko. *Differential Equations and Dynamical Systems*, chapter 3, pages 244–251. Springer, New York, NY, 2000.

[33] D.A. Roff. *Life History Evolution*, chapter Trade-offs. Sinauer, Sunderland, 2002.

[34] S.H. Strogatz. *Nonlinear dynamics and chaos*, chapter Limit Cycles, pages 196–241. Perseus Books Publishing, L.L.C., 1994.

[35] C.J.M. Thomsen and R. Sargent. Evidence that a herbivore tolerance response affects selection on floral traits and inflorescence architecture in purple loosestrife (*Lythrum salicaria*). *Annals of Botany*, 119:1295–1303, 2017.

[36] D. Waxman and S. Gavrilets. 20 questions on adaptive dynamics. *Journal of Evolutionary Biology*, 18:1139–54, 2005.

[37] A.E. Weis and T.M. Kossler. Genetic variation in flowering time induces phenological assortative mating: quantitative genetic methods applied to brassica rapa. *Americal Journal of Botany*, 91:825–836, 2004.

[38] A.E. Weis, J. Winterer, C. Vacher, T.M. Kossler, C.A. Young, and G.L. LeBuhn. Phenological assortative mating in flowering plants: the nature and consquences of its frequency dependence. *Evolutionary Ecology Research*, 7:161–181, 2005.